Science of the Total Environment 803 (2022) 149918

Contents lists available at ScienceDirect

Science of the Total Environment

journal homepage: www.elsevier.com/locate/scitotenv

Review

Co-sorption of metal ions and inorganic anions/organic ligands on environmental minerals: A review

Yupeng Yan [a,b], Biao Wan [c,*], Muammar Mansor [c], Xiaoming Wang [b], Qin Zhang [a], Andreas Kappler [c,d], Xionghan Feng [b,*]

[a] Key Laboratory of Poyang Lake Watershed Agricultural Resources and Ecology of Jiangxi Province, College of Land Resources and Environment, Jiangxi Agricultural University, Nanchang 330045, People's Republic of China
[b] Key Laboratory of Arable Land Conservation (Middle and Lower Reaches of Yangtze River), Ministry of Agriculture and Rural Affairs, College of Resources and Environment, Huazhong Agricultural University, Wuhan 430070, People's Republic of China
[c] Geomicrobiology, Center for Applied Geosciences, University of Tuebingen, 72076 Tuebingen, Germany
[d] Cluster of Excellence: EXC 2124: Controlling Microbes to Fight Infections, Tübingen, Germany

HIGHLIGHTS

- This review summarizes co-sorption characteristics and mechanisms of metals and anions/ligands on minerals.
- Promotive and competitive effects are described along with the specific molecular mechanisms.
- Co-sorption mechanisms are affected by mineral properties, sorbate species, and reacting conditions.
- Environmental impacts of metal–anion/ligand co-sorption on minerals are evaluated.
- Potential challenges and future topics for co-sorption research are discussed.

GRAPHICAL ABSTRACT

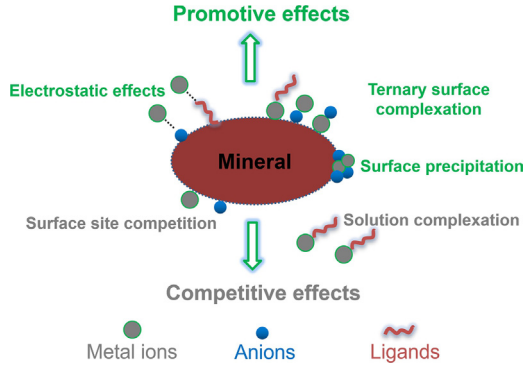

ARTICLE INFO

Article history:
Received 30 May 2021
Received in revised form 31 July 2021
Accepted 22 August 2021
Available online 26 August 2021

Editor: Baoliang Chen

Keywords:
Environmental minerals
Anions/ligands
Metal cations
Co-sorption behavior
Interaction mechanisms

ABSTRACT

Co-sorption of metal ions and anions/ligands at the mineral–water interface plays a critical role in regulating the mobility, transport, fate, and bioavailability of these components in natural environments. This review focuses on co-sorption of metal ions and naturally occurring anions/ligands on environmentally relevant minerals. The underlying mechanisms for their interfacial reactions are summarized and the environmental impacts are discussed. Co-sorption mechanisms of these components depend on a variety of factors, such as the identity and properties of minerals, pH, species and concentration of metal ions and anions/ligands, addition sequence of co-sorbed ions, and reaction time. The simultaneous presence of metal ions and anions/ligands alters the initial sorption behaviors with promotive or competitive effects. Promotive effects are mainly attributed to surface electrostatic interactions, ternary surface complexation, and surface precipitation, especially for the co-sorption systems of metal ions and inorganic anions on minerals. Competitive effects involve potential complexation of metal–anions/ligands in solution or their competition for surface adsorption sites. Organic ligands usually increase metal ion sorption on minerals at low pH via forming ternary surface complexes or surface precipitates, but inhibit metal ion sorption via the formation of aqueous complexes at high pH. The different mechanisms may act simultaneously during metal ion and

* Corresponding authors.
E-mail addresses: biao.wan@uni-tuebingen.de (B. Wan), fxh73@mail.hzau.edu.cn (X. Feng).

https://doi.org/10.1016/j.scitotenv.2021.149918

anion/ligand co-sorption on minerals. Finally, the potential application for remediation of metal-contaminated sites is discussed based on the different co-sorption behaviors. Future challenges and topics are raised for metal–anion/ligand co-sorption research.

Contents

1. Introduction

Natural and artificial environments are multicomponent systems consisting of metal ions, anions and ligands, with mutual influence on each component's environmental behavior. For example, heavy metals (e.g., cadmium (Cd), copper (Cu), lead (Pb), and zinc (Zn)) and oxyanions (e.g., arsenate (AsO_4^{3-}) and sulfate (SO_4^{2-})) have been found at extremely high concentrations in mine and timber treatment sites and wastewaters from smelting and heavy industries (Smith et al., 1998; Nakajima et al., 2011; Bian et al., 2012). Their co-presence represents a huge challenge for environmental scientists who seek effective but simple strategies for the remediation of multicomponent systems.

Sorption reactions at the mineral–water interface play a critical role in regulating the solubility, mobility, transport, fate, and biological uptake of metal ions and naturally occurring anions/ligands in the environments, which are of high relevance for global biogeochemical processes (Sparks, 2005, 2014; Putnis and Ruiz-Agudo, 2013; Kumar et al., 2014a, b). Anions and ligands can substantially affect the sorption of metal ions onto surfaces, and the same is true vice versa (Elzinga et al., 2001; Zhang and Peak, 2007; Elzinga and Kretzschmar, 2013; Zhu et al., 2019). Understanding co-sorption interactions between these components on environmentally relevant minerals are of crucial importance from environmental perspectives (Juang and Chung, 2004; Lin et al., 2004; X. Ren et al., 2012).

The molecular-level mechanisms of metal and anion/ligand interactions on environmentally relevant minerals have been studied through macroscopic sorption experiments (e.g., sorption isotherms, sorption kinetics, etc.) combined with advanced spectroscopic techniques and models, such as X-ray absorption spectroscopy (XAS), in situ attenuated total reflectance Fourier transform infrared (ATR-FTIR) spectroscopy, nuclear magnetic resonance (NMR) spectroscopy, density functional theory (DFT) calculations, and surface complexation modeling. The sorption of these species can be either promoted or inhibited via their interactions on mineral surfaces as well as in solution, which is influenced by the physicochemical properties of the mineral, pH range, surface coverage, and species and concentration of metal ions and anions/ligands (Elzinga et al., 2001; Wang and Xing, 2002, 2004; Swedlund et al., 2009; Elzinga and Kretzschmar, 2013).

The promotive effects of co-sorption are commonly attributed to one of the following reasons, or a combination of them: (1) surface electrostatic effects; (2) ternary surface complexation; and (3) surface precipitation of metal–anion/ligand species (Elzinga et al., 2001; Taylor et al., 2009; Elzinga and Kretzschmar, 2013; Ren et al., 2015), as indicated in Fig. 1. In heavy metal-contaminated soils, metal ions and anions/ligands could be co-sorbed or even converted into surface precipitates, leading to immobilization of both metal ions and anions/ligands. This promotive effect could eventually result in a decreased availability and eco-toxicity of metal ions and anions/ligands, especially for systems containing heavy metals and phosphate (PO_4^{3-}) (Hafsteinsdóttir et al., 2015; Yu et al., 2017; Zeng et al., 2017).

Competitive effects resulting in a decrease in metal sorption can be attributed to (1) the competition between aqueous metal–anion/ligand complexation and metal surface complexation on minerals, or (2) to the direct competition of surface coordination sites between metal cations and anions/ligands (Benjamin and Leckie, 1982; Theis and West, 1986; Elzinga et al., 2001; Elzinga and Kretzschmar, 2013), as shown in Fig. 1. In this case, the presence of anions/ligands may

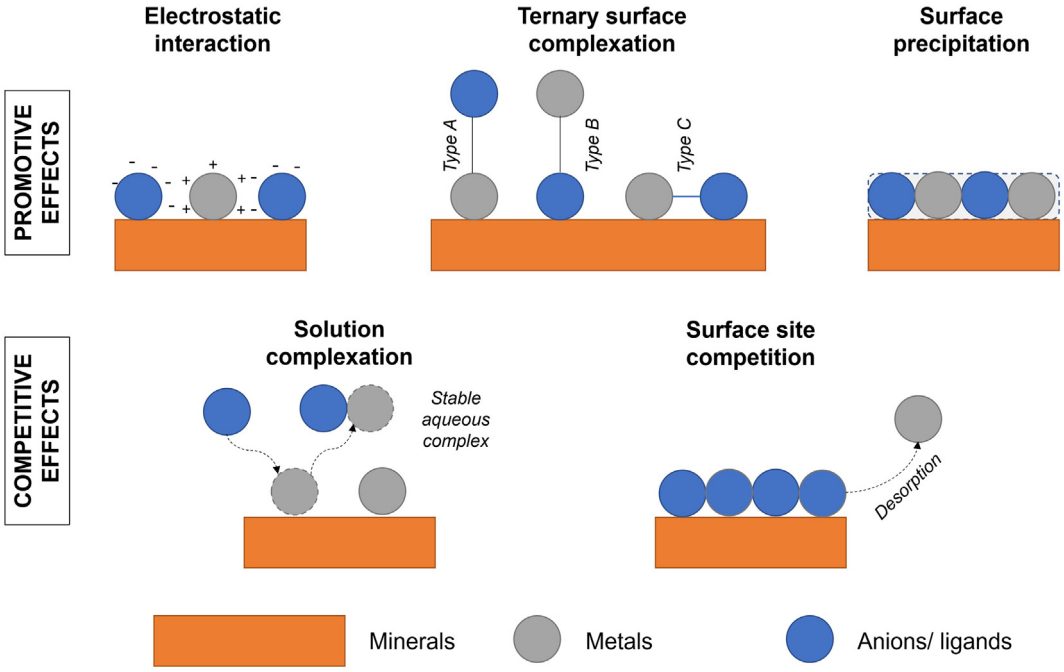

Fig. 1. Schematic diagram of co-sorption mechanisms of metal ions and anions/ligands on minerals. The co-presence of metal ions and anions/ligands can affect each other's sorption behaviors on mineral surface through promotive or competitive effects. Promotive effects are commonly attributed to surface electrostatic interactions, formation of ternary surface complexes, and surface precipitation. Depending on the coordination structures of the metal ion and anion/ligand relative to the mineral surface, the ternary complexes can be further classified into three types (A, B, and C). In type A, metal ions are near the solid surface as a metal bridge, represented as surface–metal–anion/ligand complex. In type B, the anions/ligands are located near the surface as an anion/a ligand bridge, represented as surface–anion/ligand–metal complex. In type C, both metal ions and anions/ligands are near the surface in an approximately lateral configuration, represented as metal–surface–anion/ligand complex. Competitive effects are generally attributed to solution complexation or surface adsorption site competition.

largely enhance heavy metal mobility, thereby increasing their bioavailability and toxicity, and inhibit the sequestration of heavy metals by natural colloidal and particulate minerals (Neubauer et al., 2000; Flynn and Catalano, 2017).

Due to the various environmental factors and complicated reactions involved in metal–anion/ligand co-sorption, a full understanding towards the underlying mechanisms remains limited, which warrants a need for further investigations under different environmental conditions. Recently, a variety of studies have extensively explored the mutual effects involved in the co-sorption process of metals and anions/ligands onto minerals (Zhu et al., 2019; Liu et al., 2021). However, to the best of our knowledge, a comprehensive summary of the relevant studies on this topic is missing.

This review therefore focuses on the co-sorption of metal ions (e.g., Cu (II), Pb(II), Cd(II), and Zn(II)) and anions/ligands (e.g., phosphate, arsenate, sulfate, oxalate, citrate, phthalate, amino acids, *N*-(phosphonomethyl)glycine (PMG; also known as glyphosate), and *myo*-inositol hexaphosphate (IHP)) onto environmentally relevant minerals, e.g., ferrihydrite ($Fe_{10}O_{14}(OH)_2$), goethite (α-FeOOH), hematite (α-Fe_2O_3), γ-alumina (γ-Al_2O_3), boehmite (γ-AlOOH), and kaolinite ($Al_4[Si_4O_{10}](OH)_8$). The phenomena and potential mechanisms involved in their co-sorption are thoroughly discussed and the environmental impacts are evaluated especially in the context of potential remediation applications. Finally, future research perspectives are discussed, with the aim to inspire further developments in this promising field.

2. Co-sorption of metal ions and inorganic anions on minerals

Co-sorption mechanisms of metals and inorganic anions on minerals depend on the species of the metals/inorganic anions and the properties of the minerals, all of which influence the sorption affinities and coordination modes on mineral surfaces. Additionally, co-sorption mechanisms are also affected by the saturation state of the corresponding precipitates, which depends on the pH and concentration of the metals and inorganic anions. In this section, co-sorption mechanisms of common metal ions and inorganic anions (i.e., phosphate, arsenate, selenate, selenite, silicate, carbonate, and sulfate) are summarized.

2.1. Co-sorption of metals with phosphate

2.1.1. Co-sorption characteristics of metals with phosphate

Phosphorus (P), widely present in the environment, is an essential macronutrient for biological growth and a major contributor to eutrophication and non-point source pollution (Li et al., 2013a; X. Wang et al., 2013; Yan et al., 2014). Inorganic P is the dominant P form in natural environments. As phosphate always co-exists with metal ions in the environment, the behaviors (e.g., absorption, desorption, migration and transformation) and fate of these two species are substantially influenced by each other (Hafsteinsdóttir et al., 2015; Li et al., 2017; Zeng et al., 2017).

The presence of phosphate affects the extent and rate of sorption–desorption reactions of metal ions on mineral surfaces (Juang and Chung, 2004; Wang and Xing, 2004; Adebowale et al., 2005; Zaman et al., 2009). Generally, promotive sorption effects on minerals (e.g., goethite and lepidocrocite) are observed in the co-presence of metal ions (e.g., Zn^{2+}, Cu^{2+}, and Cd^{2+}) and phosphate (Bolland et al., 1977; Diaz-Barrientos et al., 1990; Madrid et al., 1991; Wang and Xing, 2002; Li et al., 2007). However, it was also reported that pre-sorption of phosphate inhibited the sorption of Cu^{2+} and Cd^{2+} on hematite and shifted the sorption pH window of those metals to higher pH (Li et al., 2006). Meanwhile, phosphate has been reported to inhibit Cu^{2+} sorption at a relatively low concentration, but facilitated it at high concentrations (Zhu et al., 2011). This signifies that the promotive or competitive sorption effects are dependent on the concentration as well as the ratio between the metal ions and phosphate.

2.1.2. Co-sorption mechanisms of metals with phosphate

Promotive co-sorption mechanisms of metal ions and phosphate on mineral surfaces include a combination of surface electrostatic effects,

Table 1
Interaction mechanisms of metal ion and phosphate co-sorption on various minerals.

Systems	Reaction conditions	Methodology	Co-sorption mechanisms	Reference
Ferrihydrite, Zn^{2+}, phosphate	pH: 5–8 Zn^{2+}: 0–10 mg L^{-1} P/Fe: 0, 0.05, 0.1, 0.2, and 0.4	Batch experiments	Electrostatic effects	Ghanem and Mikkelson, 1988
Lepidocrocite, Zn^{2+}, phosphate	pH: 4.7–7.1 Zn^{2+}: 15–80 mg L^{-1} Phosphate: 0–200 mg L^{-1} Lepidocrocite: 10 g L^{-1}	Batch experiments	Electrostatic effects	Diaz-Barrientos et al., 1990
MnO_2, Ca^{2+}, phosphate	pH: 2–8.5 Ca^{2+}: 0.011 M Phosphate: 10 μM MnO_2: 1 mM	SCM (triple-layer model)	Electrostatic effects	Yao and Millero, 1996
Goethite, Cd^{2+}, phosphate	pH: 4–8 Cd^{2+}: 0.25–1.0 mM Phosphate: 0.54 mM Goethite: 6 g L^{-1}	CD-MUSIC	Electrostatic effects	Venema et al., 1997
Goethite, Cd^{2+}, phosphate	pH: 4.04–5.94 Cd^{2+}: 458 ppm Phosphate: 0.84 mM Goethite: 12 g L^{-1}	EXAFS	Electrostatic effects	Collins et al., 1999
Goethite, Ca^{2+}, phosphate	pH: 4–10 Ca^{2+}: 0.1 and 0.4 mM Phosphate: 0.5 mM Goethite: 2.5–10 g L^{-1}	CD-MUSIC	Electrostatic effects	Rietra et al., 2001
Goethite, Cu^{2+}, phosphate	pH: 2.0–5.4 Cu^{2+}: 0.25 mM Phosphate: 0.25 mM Goethite: 4 g L^{-1}	Batch experiments and EXAFS	Formation of ternary complexes	Lin et al., 2004
Iron hydroxide, Ni^{2+}, phosphate	pH: 3.0–7.0 Phosphate: 0.485–3.5 mM Ni-loaded iron hydroxide: 3.3 g L^{-1}	Batch experiments and FTIR	Formation of ternary complexes	Mustafa et al., 2008
MnO_2, Cd^{2+}, phosphate	pH: 4–7 Cd^{2+}: 0.08–0.71 mM Phosphate: 1–100 mM MnO_2: 3.3 g L^{-1}	Batch experiments	Formation of type B (P-bridged) surface complex at low pH and type A (metal-bridged) surface complex at high pH	Zaman et al., 2009
Hematite, Cd^{2+}, phosphate	pH: 4.5–9 Cd^{2+}: 0–5 mM Phosphate: 25 μM Hematite: 5 g L^{-1}	ATR-FTIR	Formation of ternary complexes	Elzinga and Kretzschmar, 2013
Ferrihydrite, Cu^{2+}/Pb^{2+}, phosphate	pH: 3–10 Cu^{2+}/Pb^{2+}: 0.3–30 μM Phosphate: 0.06–0.6 mM Ferrihydrite: 0.3–3 mM	EXAFS analyses and CD-MUSIC model	Formation of ternary complexes	Tiberg et al., 2013
Hydroxy-iron-montmorillonite complex, Cd^{2+}, phosphate	pH: 5 Cd^{2+}: 50–350 mg L^{-1} Phosphate: 30–120 mg L^{-1} Hydroxyiron-montmorillonite complex: 5 g L^{-1}	XPS	Formation of type B ternary complexes	Zhu et al., 2014
Ferrihydrite, Cd^{2+}, phosphate	pH: 3–7.5 Cd^{2+}: 0.3–30 μM Phosphate: 0.06–0.6 mM Ferrihydrite: 3 mM	EXAFS and SCM	Formation of ternary complexes	Tiberg and Gustafsson, 2016
Hydrous zirconium oxide, Ca^{2+}, phosphate	pH: 4–9 Ca^{2+}: 1 mM Phosphate: 5–50 mg L^{-1} Hydrous zirconium oxide: 0.4 g L^{-1}	^{31}P NMR and XPS	Formation of type B ternary complexes	Lin et al., 2017
Goethite, Ca^{2+}, phosphate	pH: 3–10 Ca^{2+}: 0.01 and 0.05 mM phosphate: 30 μM Goethite: 0.25 g L^{-1}	SCM model	Formation of calcium phosphate surface precipitates	Hawke et al., 1989
Kaolinite, Pb^{2+}, phosphate	pH: 4–10 Pb^{2+}: 0.189 mM phosphate: 3 mg L^{-1} Kaolinite: 0.5 g L^{-1}	XANES	Formation of surface precipitates similar to pyromorphite	Taylor et al., 2009
Kaolinite, Zn^{2+}, phosphate	pH: 4.5–7.5 Zn^{2+}: 1.5 mM phosphate: 1.5 mM Kaolinite: 20 g L^{-1}	EXAFS	Formation of zinc phosphate surface precipitates	Stietiya et al., 2011
Boehmite, Ca^{2+}, phosphate	pH: 6–9 Ca^{2+}: 10 mM phosphate: 1 mM Boehmite: 4.9 g L^{-1}	NMR and XRD	Formation of hydroxylapatite	Li et al., 2012
γ-Al_2O_3, Cu(II), phosphate	pH: 3–11 Cu^{2+}: 6 mg L^{-1} Phosphate: 3 mg L^{-1} γ-Al_2O_3: 1 g L^{-1}	Batch experiments and DFT calculations	Formation of type B ternary complexes and surface precipitates	X. Ren et al., 2012
Aluminum oxide nanoparticles, Zn^{2+}/Cd^{2+}, phosphate	pH: 6.5 Zn^{2+}/Cd^{2+}: 0.05–1 mM Phosphate: 0–2 mM Aluminum oxide nanoparticles: 1 g L^{-1}	Batch experiments and XPS	Formation of ternary complexes and surface precipitates	Stietiya and Wang, 2014
Ferrihydrite, Ca^{2+}, phosphate	pH: 3–10 Ca^{2+}: 0.3–6 mM Phosphate: 0.6 mM Ferrihydrite: 1 g L^{-1}	SCM model	Formation of ternary complexes and surface precipitates	Antelo et al., 2015
Hematite/goethite, Fe^{2+}, phosphate	pH: 3–9 Fe^{2+}: 0.1 and 1.0 mM Phosphate: 0.1 and 1.0 mM Hematite/goethite: 4 g L^{-1}	ATR-FTIR and SCM model	Electrostatic effects and formation of ternary complexes	Hinkle et al., 2015
γ-Al_2O_3, Zn^{2+}, phosphate	pH: 6.5 and 8 Zn^{2+}: 0.15 and 0.19 mM Phosphate: 0–0.48 mM γ-Al_2O_3: 2 g L^{-1}	Batch experiments and EXAFS	Electrostatic interaction, binary and ternary surface complexation, and the formation of Zn(II)-phosphate polynuclear complexes	Ren et al., 2015
Ferrihydrite, Zn^{2+}, phosphate	pH: 3.5–6 Zn^{2+}: 0.038–2.4 mM Phosphate: 0.081–5.2 mM Ferrihydrite: 2.5 g L^{-1}	XPS and ATR-FTIR	Formation of ternary complexes, electrostatic interactions, and surface precipitation	Liu et al., 2016

Table 1 (*continued*)

Systems	Reaction conditions	Methodology	Co-sorption mechanisms	Reference
Ferrihydrite, Cd^{2+}, phosphate	pH: 5–9 Cd^{2+}: 0.2–2 mM Phosphate: 0.5–2 mM Ferrihydrite: 2.5 g L^{-1}	ATR-FTIR	Electrostatic effects and formation of ternary complexes	Liu et al., 2018
Ferrihydrite/goethite/hematite, Cd^{2+}, phosphate	pH: 3–7 Cd^{2+}: 0.125–2 mM Phosphate: 0.125–2 mM Ferrihydrite/goethite/hematite: 0.4, 2.5, and 4 g L^{-1}	ATR-FTIR	Electrostatic interactions, formation of phosphate-bridged ternary complexes and surface precipitates	Liu et al., 2021

Abbreviations

ATR-FTIR: attenuated total reflectance Fourier transform infrared spectroscopy;
CD-MUSIC: charge distribution multi-site complexation;
DFT: density functional theory;
EXAFS: extended X-ray absorption fine structure spectroscopy;
NMR: nuclear magnetic resonance spectroscopy;
SCM: surface complexation model;
XANES: X-ray absorption near edge structure spectroscopy;
XPS: X-ray photoelectron spectroscopy.
XRD: X-ray diffraction.

ternary surface complexation and surface precipitation, as will be discussed below.

2.1.2.1. Surface electrostatic effects. The adsorption of phosphate from solution onto mineral surfaces involves both physical and chemical forces. Physical forces include van der Waals (e.g., partitioning) and electrostatic interactions which are responsible for outer-sphere complexation (e.g., ion exchange). Electrostatic bonding can occur via cation or anion exchange, or protonation. Short-range chemical interactions include inner-sphere complexation, involving surface hydroxyl exchange, covalent bonding, and hydrogen bonding mechanisms (Sparks, 2002). Surface electrostatic effects tend to promote the co-sorption of metals and phosphate on minerals. The mechanism involves the alteration of mineral surface charge due to inner-sphere ion adsorption being partially offset by the (inner-sphere) co-adsorption of ions with opposite charge. This facilitates further adsorption (relative to binary systems) by lowering the electrostatic barrier for the approach of ions to the surface (Elzinga et al., 2001; Taylor et al., 2009; Elzinga and Kretzschmar, 2013; Ren et al., 2015).

Promotive co-adsorption by electrostatic effects is considered to be the dominant mechanism for the following co-adsorption systems (Table 1): Zn^{2+}–PO_4^{3-} on ferrihydrite (Ghanem and Mikkelson, 1988) and lepidocrocite (Diaz-Barrientos et al., 1990); Ca^{2+}–PO_4^{3-} on manganese oxide (MnO_2) (Yao and Millero, 1996) and goethite (Rietra et al., 2001); Cd^{2+}–PO_4^{3-} on goethite (Venema et al., 1997; Collins et al., 1999); and Pb^{2+}–PO_4^{3-} on goethite (Xie and Giammar, 2007). For example, Diaz-Barrientos et al. (1990) found that co-sorbed phosphate increased Zn^{2+} adsorption on lepidocrocite by reducing the electrostatic potential near the mineral surface. In addition, Collins et al. (1999) reported that phosphate increased Cd^{2+} adsorption levels on goethite. However, no noticeable differences were observed in the Cd K-edge extended X-ray absorption fine structure (EXAFS) spectra in the presence or absence of co-sorbed phosphate. Particularly, the EXAFS spectra of Cd^{2+} sorbed on goethite in the presence of phosphate only showed a first shell with 6 ± 1 O atoms at 2.3 ± 0.1 Å, consistent with Cd^{2+} sorbed directly to goethite. Second shells of O and P (particularly between 3 and 3.6 Å) that are indicative of cadmium-phosphate phases were not visible in the EXAFS spectrum. Based on these observations, it was concluded that phosphate promoted Cd^{2+} adsorption mainly through electrostatic effects, rather than the formation of ternary complexes or surface precipitates. This conclusion was supported by the charge distribution multisite complexation (CD-MUSIC) model (Venema et al., 1997). Rietra et al. (2001) also showed that the adsorption and interaction of Ca^{2+} and PO_4^{3-} on goethite can be predicted by the CD-MUSIC model solely based on electrostatic effects. However, these studies usually used model parameters derived from single-ion systems and without considering ternary complexation and surface precipitation.

2.1.2.2. Ternary surface complexation. Ternary surface complexation is another main mechanism to explain promotive co-sorption of metals ions and phosphate on minerals (Elzinga et al., 2001; Elzinga and Kretzschmar, 2013). The formation of ternary metal–ligand complexes at the mineral surface increases the stability of adsorbed ionic complexes through physical or chemical bonds. Depending on the coordination structures of the metal ion and ligand relative to the solid surface, the ternary complexes can be further classified into three types (A, B, and C), as indicated in Fig. 1. In type A, metal ions are near the solid surface as a metal bridge, represented as surface–metal–anion/ligand complex. In type B, the anions/ligands are located near the surface as an anion/a ligand bridge, represented as surface–anion/ligand–metal complex. In type C, both metal ions and anions/ligands are near the surface in an approximately lateral configuration, represented as metal–surface–anion/ligand complex (Taylor et al., 2009; Ren et al., 2015).

Solution pH significantly influences the type of ternary complexes that formed on minerals. Elzinga and Kretzschmar (2013) found that the addition of Cd^{2+} ions increased the amount of phosphate adsorbed on hematite in a pH-dependent manner over a pH range of 4.5–9. Based on distinct differences between the IR spectra of Cd(II)-phosphate precipitates and ternary complexes (calculated by subtracting the spectra of adsorbed phosphate collected before Cd(II) addition from the spectra of co-sorbed phosphate recorded after Cd(II) addition), bulk precipitation did not occur in the Cd^{2+}/phosphate co-sorption system. Systematic and gradual alterations were observed in the ternary IR difference spectra when solution pH decreased from 9.0 to 4.5, suggesting the presence of at least two different Cd(II)-phosphate ternary complexes that changed proportion with pH. Principal component analysis of the ATR-FTIR difference spectra revealed that the formation of type A (Cd-bridged) ternary complexes was the dominant mechanism at high pH, while type B (phosphate-bridged) ternary complexes was the main surface species on hematite at low pH. The proposed arrangements of Cd (II)–phosphate ternary complexes are shown in Fig. 2. Similarly, Zaman et al. (2009) suggested that phosphate promoted Cd^{2+} sorption on MnO_2 minerals via the formation of type A complexes at high pH and type B complexes at low pH.

Numerous studies have shown that the type of ternary surface complexes formed on minerals depends on the reaction conditions (Table 1). For example, EXAFS analyses indicated that Cu—Fe and Pb—Fe distances become longer in the presence of phosphate on ferrihydrite. Combined with CD-MUSIC model analysis, the study suggested that the promotive sorption of Cu^{2+} and Pb^{2+} on ferrihydrite in the presence of phosphate was most probably attributed to the formation of two ternary metal–phosphate complexes (Fig. 3): (1) a surface

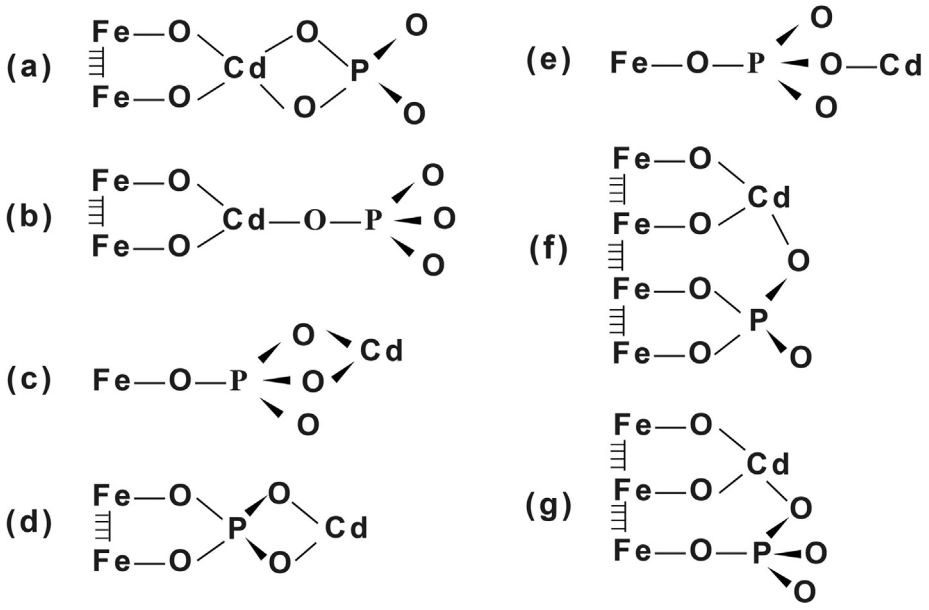

Fig. 2. Proposed configurations of Cd(II)–phosphate ternary complexes on the surface of hematite, modified from Elzinga and Kretzschmar (2013). Ternary complexation includes Cd(II)-bridged type A complexes (configuration a & b), phosphate-bridged type B complexes (configuration c, d, and e), and type C complexes with lateral interactions (configuration f & g).

complex of type C, where both metal and phosphate interact in a monodentate fashion with the ferrihydrite surface (composition $\equiv(FeO)_2HMePO_3H^0$), and (2) a corner-sharing ferrihydrite–metal complex, in which the phosphate ion is bound to the metal but not to the mineral surface, resulting in a type A complex with $\equiv(FeOH)_2$–Me–H_2PO_4 composition (Tiberg et al., 2013). EXAFS spectra of the solid products in the absence of phosphate were best fitted with two different Cd—Fe distances: the formation of bidentate complexes where a 3.3 Å distance was determined for an edge-sharing and 3.7 Å for a corner-sharing complex, respectively. Higher-shell contributions

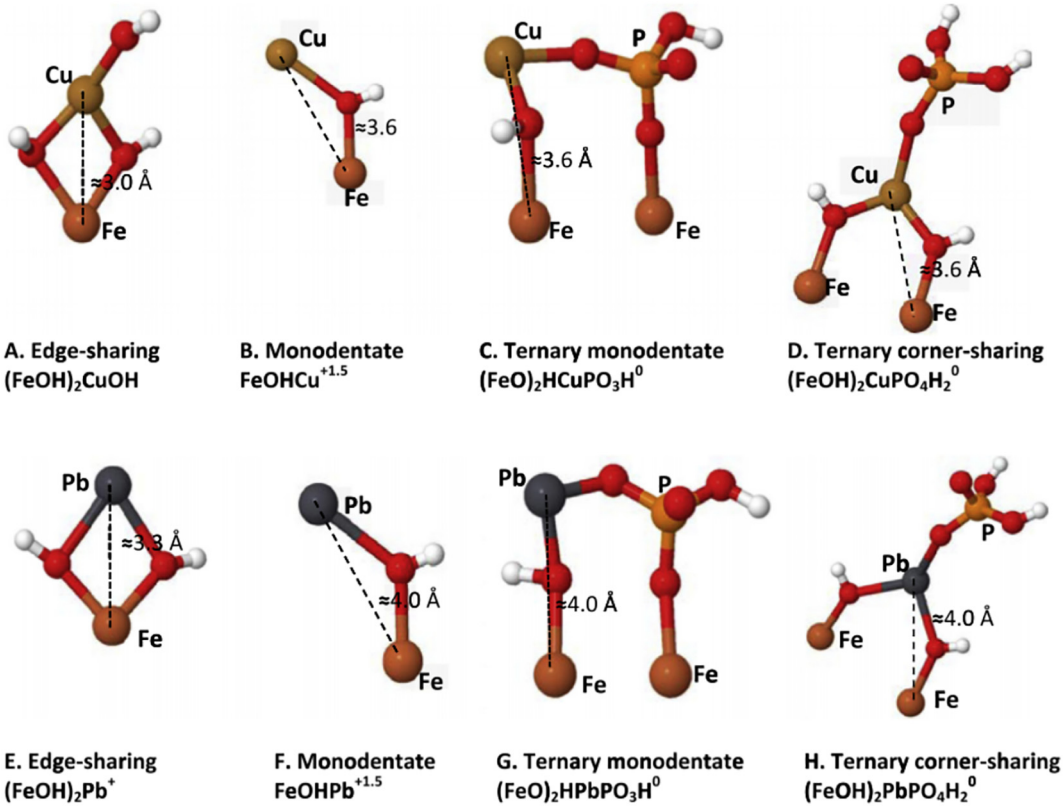

Fig. 3. Configurations of Cu(II) (top row) and Pb(II) (bottom row) complexes on ferrihydrite in the presence of phosphate. Red spheres denote oxygen atoms and white spheres denote hydrogen atoms. Iron, Cu(II), Pb(II) and phosphorus (P) atoms are marked in the figures along with the distances for the Cu···Fe and Pb···Fe bonds (Tiberg et al., 2013). (For interpretation of the references to colour in this figure legend, the reader is referred to the web version of this article.)

in phosphate-containing products were best fitted with a Cd—Fe distance at ~3.8 Å and a Cd—P distance at ~3.4 Å. Therefore, it was proposed that the formation of ternary complexes resulted in the enhanced sorption of Cd^{2+} on ferrihydrite in the presence of phosphate, which was further supported by CD-MUSIC modeling (Tiberg and Gustafsson, 2016).

Batch experiments and EXAFS analysis showed that the formation of goethite–Cu(II)–phosphate complexes (type A) increased the sorption density of both Cu^{2+} and phosphate (Lin et al., 2004). A combination of batch sorption and XPS results suggested that co-sorbed Cd^{2+} ions and phosphate formed phosphate-bridged ternary complexes (type B) on hydroxy-iron–montmorillonite surfaces, contributing to the promotive sorption of Cd^{2+} and PO_4^{3-} (Zhu et al., 2014). Similarly, the presence of Ca^{2+} substantially enhanced the sorption of phosphate on hydrous zirconium oxide (HZO) over a pH range of 6–9 via the formation of phosphate-bridged ternary complexes (≡Zr–P–Ca) (Lin et al., 2017).

2.1.2.3. Surface precipitation. Surface precipitation is the third mechanism that could account for promotive co-sorption of co-existing metal ions and phosphate on minerals. This mechanism involves the formation of a three-dimensional surface phase containing both metal ions and anions/ligands, leading to accumulations of the respective components (Elzinga et al., 2001; Taylor et al., 2009; Elzinga and Kretzschmar, 2013; Ren et al., 2015). For example, metal–phosphate precipitates could form from oversaturated solutions by concentrating their contents on the mineral surface. Given their inherently small particle size, surface precipitates are difficult to identify by conventional X-ray diffraction and scanning electron microscopy. However, it can be effectively identified via EXAFS spectroscopy (Taylor et al., 2009).

Many studies have detected the formation of metal–phosphate precipitates on mineral surfaces (Table 1). For example, Hawke et al. (1989) showed that Ca^{2+} ions increased the amount of phosphate sorption on goethite at medium to high pH through the formation of calcium phosphate surface precipitates. Li et al. (2012) performed batch sorption experiments to investigate the effect of dissolved Ca^{2+} on phosphate sorption by boehmite as a function of pH and found that the crystallization rate of hydroxyapatite was enhanced on the boehmite surface. This was also supported by thermodynamic calculations, where solutions containing 1 mM [PO_4^{3-}] and 10 mM [Ca^{2+}] were oversaturated with respect to hydroxyapatite at pH > 5.4. Weesner and Bleam (1998) performed EXAFS analysis of Pb^{2+} and phosphate co-sorption on goethite or boehmite and observed a strong similarity between the spectra of lead-phosphate model compounds and the spectra of the Pb^{2+}-phosphate co-sorption samples, suggesting the formation of lead phosphate surface precipitates (mainly as hydroxypyromorphite, $Pb_5(PO_4)OH$). Additionally, pre-sorbed phosphate considerably increased Pb^{2+} sorption density on the phyllosilicate kaolinite in the pH range of 4–8. X-ray absorption near edge structure (XANES) analysis showed that the sorbed phosphate reacted with dissolved Pb^{2+} to form surface precipitates similar to pyromorphite (Taylor et al., 2009). Furthermore, phosphate surface precipitates were detected through EXAFS analysis in the following co-sorption systems: Zn^{2+}–PO_4^{3-} on kaolinite (Stietiya et al., 2011) and lanthanide cations (Eu^{3+}, Gd^{3+}, and Dy^{3+}) co-sorbed with PO_4^{3-} on boehmite (Yoon et al., 2002).

2.1.2.4. Combination of multiple mechanisms. In most situations, the co-sorption of metal ions and phosphate on minerals involves a combination of multiple mechanisms. For example, surface electrostatic effects and ternary complex formation are considered the dominant mechanisms in the following systems (Table 1): Fe^{2+}–PO_4^{3-} on Fe(III) oxides (Hinkle et al., 2015), Zn^{2+}–PO_4^{3-} on ferrihydrite (Liu et al., 2016), Cd^{2+}–PO_4^{3-} on ferrihydrite (Liu et al., 2018), and Mg^{2+} and Ca^{2+} co-adsorbed with PO_4^{3-} on ferrihydrite (Mendez and Hiemstra, 2020). Co-sorption experiments showed a promotive effect for Fe^{2+} and phosphate adsorption on iron (oxyhydr)oxide surfaces. The IR spectra of phosphate adsorbed onto hematite and goethite in the presence of Fe(II) were clearly distinctive from that of vivianite ($Fe_3(PO_4)_2 \cdot 8H_2O$). A new IR band observed in the goethite system and a possible shift of this IR band associated with the bidentate surface complex in the hematite system with the addition of Fe(II) were observed. Below pH 6, the addition of ternary complexes to a surface complexation model (SCM) model substantially improved the model predictions in relation to the wet chemistry data. ATR-FTIR and SCM analyses indicated that the co-operative adsorption of aqueous Fe(II) and phosphate likely involved a combination of ternary complexation and electrostatic interactions (Hinkle et al., 2015).

Ternary surface complexation and surface precipitation are the dominant mechanisms in the following co-sorption systems: Zn^{2+} and Cd^{2+} co-sorbed with PO_4^{3-} on aluminum oxide nanoparticles (Stietiya and Wang, 2014), Ca^{2+}–PO_4^{3-} on ferrihydrite (Antelo et al., 2015), and Cu^{2+}–PO_4^{3-} on γ-Al_2O_3 (X. Ren et al., 2012). For example, Stietiya and Wang (2014) found that Zn^{2+} had higher sorption affinity for the surface of aluminum oxide nanoparticles than Cd^{2+}. The amounts of adsorbed Zn^{2+} and Cd^{2+} in the binary-metal system were lower than those in the respective single-metal systems, and the presence of phosphate promoted Zn^{2+} and Cd^{2+} sorption in all systems. Removal of Zn^{2+} or Cd^{2+} was generally accompanied by phosphate removal, implying that the enhanced sorption of metal ions was due to formation of ternary complexes or metal–ligand surface precipitates.

The concentrations of the metal ions and phosphate have obvious impacts on the co-sorption mechanisms. At low concentrations of metal ions and phosphate, ternary surface complexation dominates; at high concentrations, supersaturation is achieved and surface precipitation can occur. In many cases, even if the concentrations of metals and anions/ligands are below those required for bulk precipitation, surface-promoted co-sorption can still lead to the formation of surface precipitates due to local oversaturation. For instance, Antelo et al. (2015) showed promotive sorption of Ca^{2+} and phosphate on ferrihydrite in their co-presence. At low Ca^{2+} loadings, enhanced sorption of phosphate could be attributed to the formation of calcium–phosphate ternary surface complexes, as predicted by modeling simulation. However, at high Ca^{2+} loadings, the enhanced sorption of phosphate might result from the formation of ternary complexes or surface precipitates. Based on the saturation index calculation for the least soluble phosphate–calcium mineral (hydroxyapatite, $Ca_5(PO_4)_3OH$, $\log K_{sp\ (\text{solubility product})} = -58.2$), even bulk precipitation can occur at high Ca^{2+} loadings as observed in this study. X. Ren et al. (2012) reported that co-existing phosphate ions promoted Cu^{2+} sorption on γ-Al_2O_3, whereas phosphate sorption was not affected by the co-existing Cu^{2+} at low initial phosphate concentrations. Nevertheless, phosphate sorption was enhanced in the presence of Cu^{2+} at high initial phosphate concentrations, which could be attributed to the formation of 1:2 Cu(II)–phosphate species and/or surface precipitates. The relative energy of type B ternary surface complexes was lower than that of type A complexes, suggesting that the formation of type B ternary surface complexes was more favorable from a thermodynamic aspect. In another study, Ren et al. (2015) found that the Zn K-edge XANES spectrum of a Zn-phosphate co-sorption sample was different from that of $Zn_3(PO_4)_2$, indicating that the formation of Zn-phosphate precipitate did not occur in the presence of γ-Al_2O_3. Speciation calculation indicated that the solution was undersaturated with respect to $Zn_3(PO_4)_2$ precipitates. Multiple mechanisms were found to control Zn^{2+} retention on γ-Al_2O_3 in the presence of phosphate, including electrostatic interactions, binary and ternary surface complexation, and formation of Zn(II)–phosphate polynuclear complexes, depending on the solution pH and phosphate concentration.

Mineral properties (e.g., crystallinity, specific surface area, and particle size) are other important factors affecting the co-sorption mechanisms. Even for a same mineral, there can be variations in the crystallinity, morphology, shapes, and defects that affect mineral surface reactivity and sorption mechanisms. Among different iron (oxyhydr)

oxides, ferrihydrite is of particular interest because of its poor crystallinity, large specific surface areas, and high reactivity (Kappler et al., 2021). The amount of sorbed metal ions and anions (e.g., phosphate) on ferrihydrite is much higher than those on other, more crystalline iron (oxyhydr)oxides, such as hematite and goethite (X. Wang et al., 2013). Recently, Liu et al. (2021) reported that the sorption of Cd^{2+} and phosphate on ferrihydrite, goethite, and hematite was controlled by similar promotive mechanisms, including electrostatic interactions, formation of phosphate-bridged ternary complexes, and surface precipitation. However, the relative contributions of these mechanisms were different for these three minerals: electrostatic attraction was the predominant co-sorption mechanism on goethite, while surface precipitation was most significant on ferrihydrite. These studies indicate that the interfacial mechanisms of metal and phosphate co-sorption depend on the mineral properties (Liu et al., 2021).

2.1.3. Co-sorption of U(VI) with phosphate

Uranium (U) is a natural radionuclide that can be enriched in certain localities due to human activities (e.g., nuclear plants), and its sorption behavior is one of the key geochemical processes that governs its mobility and toxicity (Comarmond et al., 2016). Uranium remediation at contaminated field sites typically involves the usage of phosphate salts or phosphate-containing minerals (Mehta et al., 2016; Zhang et al., 2020). Thus, this separate subsection is included to address U and phosphate co-sorption.

Solution pH is a crucial factor that affects the role of phosphate regarding U(VI) sorption. At low pH values, the amount of U(VI) adsorbed on goethite increases in the presence of phosphate, and phosphate is strongly bound to the goethite surface, which was attributed to the formation of ternary surface complexes involving both U(VI) and phosphate. At high pH values, the amount of U(VI) adsorbed decreased in the presence of phosphate, due to the formation of dissolved U(VI)–phosphate complexes (Cheng et al., 2004).

The co-sorption mechanisms of U(VI) and phosphate on minerals are affected by the uranium and phosphate concentrations as well as their concentration ratio (Galindo et al., 2010; Singh et al., 2010, 2012; Del Nero et al., 2011; Comarmond et al., 2016; Troyer et al., 2016). For example, U(VI)–phosphate precipitates formed on goethite were detected, depending on the uranium/phosphate concentration ratio. Enhanced U(VI) sorption was observed at the highest phosphate concentration (130 μM), likely due to the formation of ternary surface complexes for low (~1 μM) to intermediate (~10 μM) uranium concentrations and the precipitation of U(VI)–phosphate species at high (~100 μM) uranium concentrations (Singh et al., 2010). In addition, promotion of U(VI) sorption on α-Al_2O_3 in the presence of phosphate was attributed to both surface complexation and precipitation, with the predominant species being mainly dependent on surface phosphate coverage (Galindo et al., 2010).

2.1.4. Soil remediation by phosphate

Considering the strong effects of phosphate on metal mobility and transport, the application of phosphate salts or phosphate-bearing minerals is considered as one of the more promising methods for remediation of metal-contaminated systems via the formation of poorly soluble metal-phosphate phases (Miretzky and Fernandez-Cirelli, 2008; Pérez-Novo et al., 2009, 2011; Mauric and Lottermoser, 2011; L. Wang et al., 2013; Huang et al., 2016; Li et al., 2017; Obrycki et al., 2017; Zhao et al., 2017). A variety of metals such as Pb^{2+}, Ba^{2+}, Cd^{2+}, Co^{2+}, Cu^{2+}, Eu^{3+}, Ni^{2+}, and Zn^{2+} can be effectively immobilized by phosphate (Hafsteinsdóttir et al., 2015). For example, at a Pb-contaminated field site, phosphate treatment remarkably reduced Pb sequestrations (reduction of 20–71%) by St. Augustine grass (*Stenotaphrum secundatum*). A mixture of H_3PO_4 and phosphate rock amendments yielded the best overall results for in-situ Pb retention and remediation, with only small changes in soil pH and low amounts of P leaching. Pb immobilization was attributed to the formation of almost insoluble chloropyromorphite ($Pb_{10}(PO_4)_6Cl_2$) (Cao et al., 2002), which has a very low K_{sp} of $10^{-84.4}$ (Zeng et al., 2017). The addition of phosphate facilitated pyromorphite formation in a concentration-dependent manner. EXAFS analysis showed that the proportion of pyromorphite in an urban soil ranged from 0% (control) to 45% (1% phosphoric acid amendment, residence time of 32 months) relative to total Pb content (Scheckel and Ryan, 2004).

Although pyromorphite formation has the potential to control Pb solubility at low levels from a thermodynamic aspect, pyromorphite formation in reality is kinetically controlled by the pH and is dependent on the solubilities of the phosphate source and the Pb species (Chrysochoou et al., 2007). Excess quantities of dissolved and acidic phosphate sources, such as phosphoric acid, are necessary for successful in-situ pyromorphite formation. Even under these conditions, EXAFS analysis showed that the conversion of Pb^{2+} to pyromorphite in in-situ-treated soils was less than 45% after 32 months. The application of lime (CaO) to restore soil pH for acidified soil treatments inhibited further precipitation, thus reducing the effectiveness of remediation.

In the case of Cu remediation via soil amendment with vivianite, the Cu^{2+} leachability assessed by a leaching procedure was reduced by 63–87%, and the Cu^{2+} concentrations in soil extracts decreased from 1.74–13.33 mg L^{-1} to 0.23–2.55 mg L^{-1} after a 56-day vivianite treatment. The bioavailability of Cu^{2+} was therefore reduced by 54–69%. The interaction of Cu^{2+} with phosphate through surface adsorption and precipitation was mainly responsible for the reduced Cu^{2+} bioavailability in soils (Liu and Zhao, 2007).

From the examples above, phosphate application is a viable remediation strategy to decrease the bioavailability and phytotoxicity of heavy metals. However, many studies have overlooked the potential for associated P leaching and potential eutrophication problems, along with other issues such as enhanced leaching of oxyanion contaminants (e.g., arsenic (As) and selenium (Se)) (Chrysochoou et al., 2007). The potential for secondary contaminations need to be strongly considered for in-situ treatment of heavy metals by different phosphate compounds.

2.2. Co-sorption of metals with arsenate or arsenite

Arsenic is one of the most common metalloid pollutants in the environment and is highly toxic to most organisms (Mohan and Pittman, 2007; Singh et al., 2015). Common As species include arsenate (AsO_4^{3-}, As(VI)) and arsenite (AsO_3^{3-}, As(III)). Their sorption–desorption characteristics and mechanisms on iron and aluminum oxides have been extensively studied (Raven et al., 1998; Masue et al., 2007; Loring et al., 2009; Li et al., 2011). In co-sorption systems, the effects on metal and/or arsenic adsorption can be promotive or competitive. For example, the presence of arsenate led to either increased adsorption of Cd(II)/Zn(II) or desorption of pre-sorbed Cd(II)/Zn(II) in a variety of soils depending on the exact environmental conditions (Liang et al., 2007a,b).

The mechanism of arsenate–metal co-sorption on minerals differs from the mechanism for arsenite sorption, because of the different sorption affinities and mechanisms of these two As species. Results from single-sorbate experiments showed that Fe(II) formed secondary Fe(II)–Al(III)-layered double hydroxide (LDH) phases, whereas As(III) and As(V) formed inner-sphere surface complexes on γ-Al_2O_3 surfaces. Same kinetics and mechanisms of Fe(II) and As(III) sorption were observed in single- and dual-sorbate experiments, indicating that the adsorption processes of Fe(II) were unaffected by arsenite and vice versa. Similarly, arsenic XAS analysis showed that the mode of As(V) sorption was not noticeably modified by the presence of Fe(II). In contrast, the rate of and extent of As(V) sorption were increased in the presence of Fe(II) in dual-sorbate experiments, possibly promoted via surface electrostatic effects. In addition, the presence of As(V) hindered the formation of Fe(II)–Al(III)–LDH

precipitates, slowing their precipitation at low As(V) concentrations and stopping the precipitation at high concentrations (Zhu and Elzinga, 2015).

Electrostatic effects are considered a dominant mechanism for many metal–arsenic co-adsorption systems. For example, the presence of Ca^{2+} ions was reported to facilitate promotive adsorption of Ca^{2+} and arsenate on ferrihydrite. The positively charged adsorbed Ca^{2+} ions promoted the adsorption of negatively charged arsenate ions by changing the surface electrostatic potential. With increasing loading of Ca^{2+} on ferrihydrite, the repulsive electrostatic interactions between the negatively charged ferrihydrite surface (at relatively high pH values) and the arsenate ions decreased. Application of a charge distribution model showed that the mutual interactions between Ca^{2+} and arsenate could be successfully described using the parameters of the single-component systems, indicating that the enhanced adsorption could be attributed solely to the changes in electrostatic forces at the solid–solution interface (Antelo et al., 2015). Similarly, the simultaneous addition of Mn(II) and As(V) into hematite suspensions resulted in increased adsorption of As(V) via electrostatic attraction within a pH range of 4–9 (H. Ren et al., 2012).

Metal cations and As species can form ternary complexes on mineral surfaces. As(V) enhanced Cu(II) sorption on goethite through the formation of type A (surface site–Cu(II)–As(V)) and type B (surface site–As(V)–Cu(II)) ternary complexes. The formation constants of $\equiv(Fe_3OFeOH)Cu_2(OH)_2HAsO_4^{1-}$ and $\equiv FeOAsO_3Cu^{0.5-}$ are $10^{-13.15}$ and $10^{-13.42}$, respectively (Nelson et al., 2013). In addition, analysis of adsorption edge and zeta potential in combination with SCM results suggested promotive adsorption effects of As(III) and Cd^{2+} on titanium oxide (TiO_2) due to the formation of type B ternary surface complex (Hu et al., 2015), as shown in Fig. 4. The same was observed for Zn(II) ions and As adsorption on magnetite nanoparticles at pH 8.0 (Yang et al., 2010).

Ternary complex formation and surface precipitation are also the dominant sorption mechanisms in a variety of co-sorption systems (Table 2), such as Cd^{2+}–AsO_4^{3-} on goethite, brushite ($Mg(OH)_2$) and TiO_2 (Jiang et al., 2013; Zhai et al., 2018; Hu et al., 2019), Cu^{2+}–AsO_4^{3-} on goethite (Gräfe et al., 2008a), Fe^{2+}–AsO_4^{3-} on goethite (Catalano et al., 2011), Ni^{2+}–AsO_4^{3-} on ferrihydrite (Wang et al., 2018), Zn^{2+}–AsO_4^{3-} on goethite, ferrihydrite, and γ-Al_2O_3 (Grafe and Sparks, 2005; Carabante et al., 2012; Wang et al., 2017), and Zn^{2+}/Cu^{2+}–AsO_4^{3-} on goethite (Gräfe et al., 2008b). Co-existing Ni(II) and As(V) species at the surface of ferrihydrite were found to form ternary As–O–Ni complexes; such multilayer surface complexes initially occurred as surface precipitates (Wang et al., 2018). In the presence of Cd(II) and As(V), mixed amorphous and crystalline precipitates were formed on brushite at pH 8 through a coupled dissolution–precipitation mechanism, as indicated by in-situ atomic force microscopy and high-resolution transmission electron microscopy (Zhai et al., 2018).

Solution pH can affect the co-sorption mechanisms. For example, different mechanisms of Cd(II) and As(V) surface interaction were involved at pH 5.0 versus at pH 7.0 on TiO_2. At pH 5.0, a Cd(II)–As(V)–TiO_2 ternary surface complex was formed followed by the formation of a layer-by-layer surface precipitate. At pH 7.0, Cd(II)–As(V) surface precipitates were directly formed via precipitation from aqueous Cd(II)–As(V) complexes (Hu et al., 2019). In another example, precipitation of zinc hydroxide carbonate at pH 8 was followed by arsenate sorption onto the precipitates, which increased arsenate removal in the presence of Zn(II). However, at pH 4, the presence of Zn(II) in the system did not obviously affect arsenate sorption on ferrihydrite (Carabante et al., 2012).

The sequence of addition of metal ions and As(V) can also affect the co-sorption mechanisms, as seen in the case of Zn and As co-sorption on γ-alumina. At pH 5.5, koettigite ($(Zn_3(AsO_4)_2\cdot 8H_2O)$)-like precipitates were formed in the co-sorption system regardless of the addition sequence of As and Zn. At pH 7.0, Zn pre-equilibration with γ-alumina before As introduction resulted in the formation of mixed Zn—Al LDH-like and amorphous adamite-like ($Zn_2(AsO_4)OH$) precipitates. However, when Zn and As were added simultaneously, only adamite-like precipitate was observed (Wang et al., 2017).

The solid/solution ratio, along with the concentration and sorption density of metal ions and As(V), is an additional key parameter affecting co-sorption behaviors. It was reported that co-sorbed Zn(II) and As(V) showed an increased amount of sorption on goethite when compared to single-sorption systems. When surface arsenate coverages were less than its saturation sorption amount on goethite, arsenate still formed surface complexes on goethite by coordinating with Fe and/or Zn ions for the Zn and arsenate co-sorption. Above the surface saturation limit, Zn and arsenate gradually formed an adamite-like surface precipitate on goethite (Gräfe et al., 2004). Furthermore, based on the coordination numbers of As(V) and Zn atoms and the Zn—As radial distance as calculated by EXAFS analysis, adamite- and koritnigite-like precipitates were inferred on goethite with relative proportion that depended on the solid/solution ratio or surface sorption density (Gräfe and Sparks, 2005). Similarly, reaction conditions affect the co-sorption of Fe(II) and arsenate on iron (oxyhydr)oxides. The presence of Fe(II) had a minimal effect on the sorption behavior of arsenate on goethite

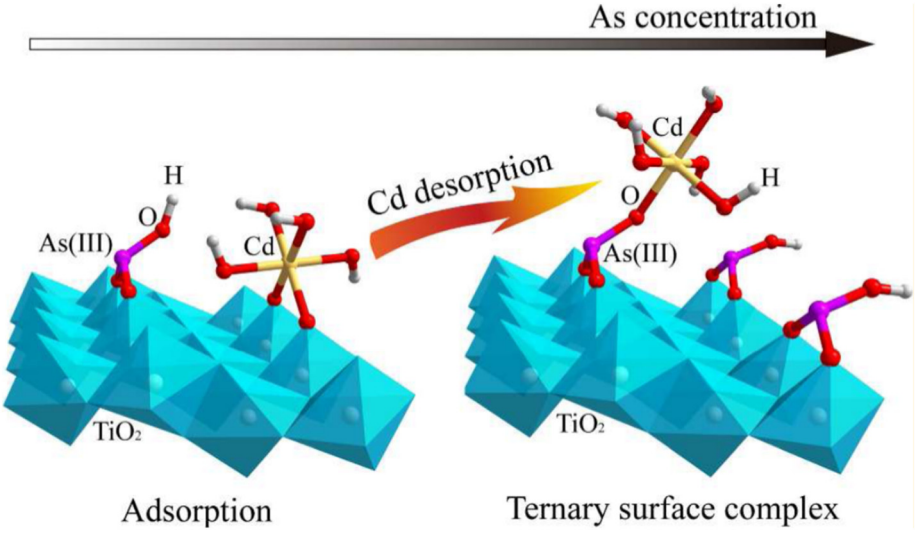

Fig. 4. Ternary surface complexation of cadmium ion (Cd^{2+}) and arsenite [As(III)] on TiO_2. At high As(III) concentration, Cd^{2+} is desorbed and re-adsorbed to the TiO_2 surface as a type B As(III)-bridged ternary complex (Hu et al., 2015).

Table 2
Interaction mechanisms of metal ion and arsenate/arsenite co-sorption on various minerals.

Systems	Reaction conditions	Methodology	Co-sorption mechanisms	Reference
Goethite, Zn^{2+}, arsenate	pH: 4 and 7 Zn^{2+}: 0.25 mM Arsenate: 0.25 mM Goethite: 1 g L^{-1}	Batch experiments	Formation of surface complexes or adamite-like precipitates, depending on As(V) surface coverage	Gräfe et al., 2004
Goethite, Zn^{2+}, arsenate	pH: 7 Zn^{2+}: 0.25 mM Arsenate: 0.25 mM Goethite: 0.01, 0.1, and 1 g L^{-1}	EXAFS	Formation of adamite-like and koritnigite-like precipitates, depending on solid/solution ratio or sorption density	Grafe and Sparks, 2005
Goethite, Cu^{2+}, arsenate	pH: 7 Cu^{2+}: 0.25 mM Arsenate: 0.25 mM Goethite: 70 m^2 L^{-1}	EXAFS	Formation of precipitates	Gräfe et al., 2008a
Goethite, Zn^{2+}/Cu^{2+}, arsenate	pH: 7 Zn^{2+}/Cu^{2+}: 0.25 mM Arsenate: 0.25 mM Goethite: 70 m^2 L^{-1}	EXAFS	Formation of clinoclase-like and koettigite-like structures	Gräfe et al., 2008b
Magnetite nanoparticles, Zn^{2+}, arsenate	pH: 4.5–8 Zn^{2+}: 1.2–3.3 mg L^{-1} Arsenate: 0.085–0.124 mg L^{-1} Magnetite nanoparticles: 0.1 g L^{-1}	Batch experiments	Formation of ternary surface complexes	Yang et al., 2010
Goethite and hematite, Fe^{2+}, arsenate	pH: 4.03–7.79 Fe^{2+}: 0.1–1 mM Arsenate: 0.1–1 mM Goethite and hematite: 4 g L^{-1}	EXAFS	Formation of ferrous arsenate precipitates (symplesite)	Catalano et al., 2011
Ferrihydrite, Zn^{2+}, arsenate	pH: 4 and 8 Zn^{2+}: 0.06 and 1.2 mM Arsenate: 0.06 mM Ferrihydrite: 0.056 g L^{-1}	ATR-FTIR	Precipitation of zinc hydroxide carbonate followed by arsenate adsorption onto the precipitate	Carabante et al., 2012
Hematite, Mn^{2+}, arsenate	pH: 4.0–8.3 Mn^{2+}: 0.267–1 mM Arsenate: 0.267 mM Hematite: 2–4 g L^{-1}	Batch experiments	Electrostatic attraction	H. Ren et al., 2012
Goethite, Cd^{2+}, arsenate	pH: 3–10 Cd^{2+}: 0.1 mM Arsenate: 0.5 mM Goethite: 2 g L^{-1}	EXAFS	Formation of ternary surface complexes and surface precipitates	Jiang et al., 2013
TiO_2, Cd^{2+}, arsenite	pH: 3–9 Cd^{2+}: 2.63–4.96 mM arsenite: 0.03–51.52 mM TiO_2: 0.2 g L^{-1}	SCM	Formation of ternary surface complexes	Hu et al., 2015
γ-Al_2O_3, Fe^{2+}, arsenate	pH: 7.5 Fe^{2+}: 1 mM Arsenate: 0.1–0.5 mM γ-Al_2O_3: 5 g L^{-1}	Batch experiments and EXAFS	Electrostatic effects	Zhu and Elzinga, 2015
Ferrihydrite, Ca^{2+}, arsenate	pH: 3–10 Ca^{2+}: 0.3–6 mM Arsenate: 0.6 mM Ferrihydrite: 1 g L^{-1}	CD-MUSIC model	Electrostatic effects	Antelo et al., 2015
γ-Al_2O_3, Zn^{2+}, arsenate	pH: 5.5 and 7.0 Zn^{2+}: 0.5–4 mM Arsenate: 1–5 mM γ-Al_2O_3: 4 g L^{-1}	Synchrotron Radiation-based X-ray Diffraction and EXAFS	Formation of Zn—Al LDH-like and amorphous adamite-like precipitates, inner-sphere complexes, and surface ternary complexes	Wang et al., 2017
Ferrihydrite, Ni^{2+}, arsenate	pH: 4.1–7.2 Ni^{2+}: 0–2.1 mM Arsenate: 0.1–0.6 mM Ferrihydrite: 0.048 g L^{-1}	ATR-FTIR	Formation of ternary surface complexes and surface precipitates	Wang et al., 2018
Brushite, Cd^{2+}, arsenate	pH: 6 and 8 Cd^{2+}: 0–0.5 mM Arsenate: 0–0.5 mM	AFM and HR-TEM	Formation of Mixed crystalline and amorphous Cd$_{(5-x)}Ca_x(AsO_4)_{(3-y)}(PO_4)_yOH$ phases	Zhai et al., 2018
TiO_2, Cd^{2+}, arsenate	pH: 3–8 Cd^{2+}: 3.11 mM Arsenate: 1.56 mM TiO_2: 1 g L^{-1}	ATR-FTIR and EXAFS	Formation of ternary surface complexes and surface precipitates	Hu et al., 2019

Abbreviations

AFM: atomic force microscopy;
ATR-FTIR: attenuated total reflectance Fourier transform infrared spectroscopy;
CD-MUSIC: charge distribution multi-site complexation;
EXAFS: extended X-ray absorption fine structure spectroscopy;
HR-TEM: high-resolution transmission electron microscopy.
SCM: surface complexation model.

and hematite at pH 4 at low concentrations of Fe(II) (0.1 mM) and arsenate (<0.5 mM). In contrast, at pH 7 and high concentrations of Fe(II) (1 mM) and arsenate (>1 mM), the ferrous arsenate mineral symplesite ($Fe_3(AsO_4)_2 \cdot 8H_2O$) has been found to form surface precipitates (Catalano et al., 2011).

Overall, the presence of metal ions could promote the retention of arsenate on minerals by electrostatic effects and the formation of ternary surface complexes and surface precipitates. From environmental remediation aspects, Fe^{2+}, Fe^{3+}, and Ca^{2+} ions are promising environmentally friendly candidates and have been applied to remediate arsenate-contaminated soils and groundwater. For example, with increasing initial concentrations of amorphous iron precipitates, extractable As (5% NaOCl) steeply decreased in As-contaminated tailings (Kim et al., 2003). In addition, after the treatment with ferrous sulfate, dissolved As concentrations in realgar ($As^{II}_4S_4$) tailing waters were reduced from 135 mg L^{-1} to below 2.5 mg L^{-1}. Addition of ferrous sulfate enhanced the transformation of Ca—As (pharmacolite ($CaHAsO_4 \cdot 2H_2O$), weilite ($CaHAsO_4$)) and S—As (realgar (As_4S_4), orpiment (As_2S_3)) species to more stable Fe—As species (e.g., crystalline symplesite and amorphous Fe—As phases) (Wang et al., 2019). Application of Fe(II)/Fe(III) could decrease the bioavailability of As, which would greatly relieve the toxicity to plants and other organisms. Amendments of $FeCl_2$ were shown to reduce grain-bound As by approximately 50% when compared to the unamended control (Yu et al., 2017).

In natural ecosystems, multiple ions and metal compounds always co-exist together. For soils that are contaminated by both heavy metals and As, comprehensive remediation measures should be undertaken. Phosphates addition to these contaminated soils decreased Pb leachability, but led to conspicuous As mobilization (Xenidis et al., 2010). Simultaneous immobilization of Pb and As could be achieved by treating soils with phosphates and ferrous sulfate at the same time (Cui et al., 2010; Xenidis et al., 2010).

2.3. Co-sorption of metals with selenate or selenite

Selenium predominantly occurs in the form of selenate (SeO_4^{2-}, Se(VI)), selenite (SeO_3^{2-}, Se(IV)), elemental Se (Se^0, Se(0)), and selenide (Se^{2-}) species (Tang et al., 2015). Aqueous Se(VI) is the fully oxidized Se species and is commonly found in aerated soils, whereas Se(IV) is a reduced state mainly observed in anoxic soils (Peak and Sparks, 2002; Kushwaha et al., 2021). It is generally accepted that Se(IV) predominantly forms inner-sphere surface complexes on iron, aluminum, and manganese (oxyhydr)oxides (Hayes et al., 1987; Foster et al., 2003; Elzinga et al., 2009; Jordan et al., 2014). Se(VI) forms only inner-sphere surface complexes on hematite, whereas a mixture of

outer- and inner-sphere Se(VI) complexes has been observed on goethite and hydrous ferric oxide surfaces (Peak and Sparks, 2002).

When Se(IV) or Se(VI) coexist with metal ions, their sorption characteristics and mechanisms are mutually affected. For example, Se(IV) substantially altered the amount of Co^{2+} sorption on γ-Al_2O_3. At low Co^{2+} surface loadings, the presence of Se(IV) ions increased Co^{2+} sorption. Co^{2+} sorption was almost unaffected at low Se(IV) coverages, but considerably increased at high Se(IV) loadings. In contrast, Se(VI) had no impact on Co^{2+} sorption. The different effects observed between Se(IV) and Se(VI) on Co^{2+} sorption were attributed to the low sorption affinity of Se(VI) on γ-Al_2O_3 when compared to Se (IV) (Boyle-Wight et al., 2002a).

EXAFS analysis revealed that the promotive effect of Se(IV) on Co^{2+} sorption was dependent on the Se(IV) surface coverage. At low Se/Co ratios on the surface, Co(II)–Al(III) LDH precipitates dominated as the surface-associated Co(II) species. Increasing the Se/Co ratio resulted in the gradual conversion of these co-precipitates to an unknown disordered Co(II)/Se(IV) phase; the latter consists of a LDH-containing interlayer Se(IV) species, an alternative precipitate such as a mixed metal selenite hydrate, or a ternary complex (Boyle-Wight et al., 2002b).

Strontium (Sr) ions also influenced the sorption of selenium species. Se(IV) formed bidentate inner-sphere surface complexes on goethite, while Sr(II) formed outer-sphere complexes at low to intermediate pH levels and inner-sphere complexes at high pH values. Instead of a direct interaction between Se(IV) and Sr(II), electrostatic interactions lead to the mutual adsorptive enhancement of Se(IV) and Sr(II). The amount of adsorbed Sr(II) increased by an average factor of 5 within the pH range from 6 to 8. However, the effect of electrostatic interactions on surface Sr(II) coverage differed based on pH: Se(IV) generally promoted the formation of Sr(II) outer-sphere complexes, but inhibited the formation of Sr(II) inner-sphere complexes at high pH values (Nie et al., 2017).

2.4. Co-sorption of metals with silicate

The ubiquitous presence of silicate (SiO_3^{2-}) in nature influences metal sorption on minerals and thus their mobility and transportation (Tan et al., 2014). For example, increasing silicate coating on γ-Al_2O_3 reduced Ni sorption. EXAFS measurements and proton dissolution experiments showed that the presence of silicate prevented the growth of Ni—Al LDH precipitates, which led to the formation of a less stable Ni—Al LDH phase (Tan et al., 2014). The presence of silicate enhanced U(VI) sorption on γ-Al_2O_3 surface through the formation of ternary inner-sphere surface complexes (Fig. 5), where silicate acted as a bridge between U(VI) and γ-Al_2O_3, or both U(VI) and silicate were near the surface in an approximately lateral configuration (Mei et al., 2015).

2.5. Co-sorption of metals with carbonate

Dissolved carbonate (CO_3^{2-}) species affect the sorption behavior of metal ions on minerals by different interfacial mechanisms (Villalobos et al., 2001). Ostergren et al. (2000b) elucidated the associated molecular-scale sorption processes by characterizing the structures of Pb(II) surface complexes on goethite in the presence of carbonate. ATR-FTIR and EXAFS analyses revealed the formation of type A ternary surface complexes on goethite, with carbonate groups bound to Pb as monodentate complexes. Formation of such species explained the promotive sorption of Pb^{2+} on goethite with elevated partial pressure of CO_2 at pH 4.5–6.5 (Ostergren et al., 2000a,b). The triple-layer model (TLM) further showed that carbonate did not affect the total sorption amounts of Pb^{2+} at the ratio studied, but led to the change of Pb(II) surface species to a predominance of ternary complexes above pH 7 (Villalobos et al., 2001). Therefore, the presence of carbonate could affect the surface speciation, transport and stability of heavy metal ions in high CO_2 environments.

2.6. Co-sorption of metals with sulfate

Sulfate (SO_4^{2-}) is another anionic species widely present in the environment especially in marine systems. A large number of studies reported that, compared to the single-sorbate systems, the presence of sulfate facilitated metal ion (e.g., Cd^{2+}, Co^{2+}, Cu^{2+}, Fe^{2+}, Hg^{2+}, Pb^{2+}, and Zn^{2+}) sorption onto minerals (e.g., goethite, ferrihydrite, γ-alumina, and hematite), especially at low pH values (Hoins, 1993; Ali and Dzombak, 1996b; Swedlund and Webster, 2001; Juang and Wu, 2002; Swedlund et al., 2003, 2009; Kim et al., 2004; Zhang and Peak, 2007; Hinkle et al., 2015).

Electrostatic effects are considered as the main mechanism for these observations (Table 3). For example, enhanced adsorption of Cd^{2+} on goethite in the presence of sulfate was solely attributed to electrostatic interactions, implying that sulfate adsorbed onto sites other than those occupied by Cd^{2+} (Collins et al., 1999). The Cu^{2+} adsorption edge shifted to a lower pH (6.3 to 5.6) in the presence of SO_4^{2-}, consistent with a reduced electrostatic repulsion between goethite surface and adsorbed Cu^{2+}. The presence of Cu^{2+} also increased SO_4^{2-} affinity on the goethite surface. ATR-FTIR spectroscopic analysis indicated the single peak in the differentiation spectra of SO_4^{2-} in the absence and presence of Cu^{2+} was assigned to the outer-sphere asymmetric stretch mode at approximately 1100 cm^{-1}, which was also observed in the Cu^{2+}-SO_4^{2-} co-sorption system. This result implied that enhanced sorption of Cu^{2+} on goethite in the presence of SO_4^{2-} was caused by electrostatic effects, rather than by forming ternary complexes (Beattie et al., 2008). Based on modeling studies, surface electrostatic effects were also proposed to account for

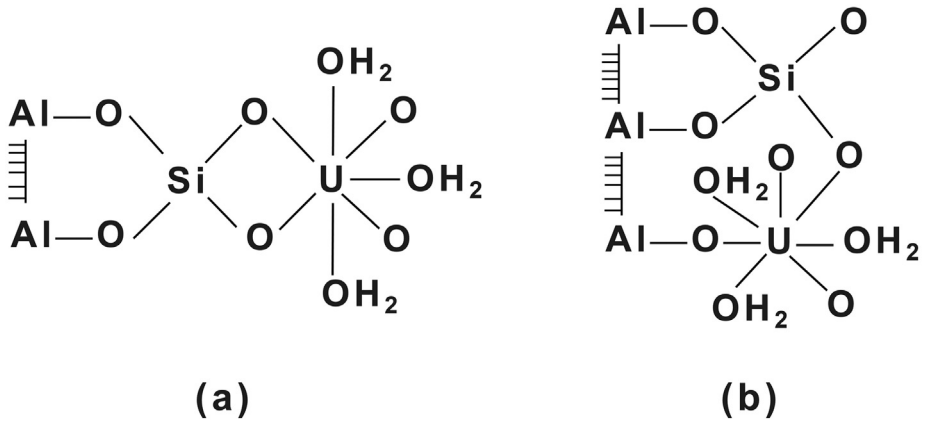

Fig. 5. Type B (a) and type C (b) ternary surface complexes of U(VI) and silicate on γ-Al_2O_3 surface. U(VI) is complexed with (a) two oxygens bound to the Si atom, or (b) two oxygens bound to a Si atom or an Al atom, respectively, modified from Mei et al. (2015).

Table 3
Interaction mechanisms of metal ion and sulfate co-sorption on various minerals.

Systems	Reaction conditions	Methodology	Co-sorption mechanisms	Reference
Goethite, Cu^{2+}, sulfate	pH: 3–9 Cu^{2+}: 0.023–0.098 mM Sulfate: 0.025–0.25 M Goethite: g L^{-1}	The generalized two-layer model	Formation of ternary complexes	Ali and Dzombak, 1996b
Goethite, Cd^{2+}, sulfate	pH: 4.6 Cd^{2+}: 403 ppm Sulfate: 4×10^{-5} M Goethite: 18 g L^{-1}	EXAFS	Electrostatic effects	Collins et al., 1999
Goethite, Pb^{2+}, sulfate	pH: 3–7 Pb^{2+}: 0.1–2.25 mM Sulfate: 0.1–3.16 mM Goethite: 1.5–5 g L^{-1}	EXAFS and ATR-FTIR	Formation of ternary complex	Ostergren et al., 2000a
Goethite, Pb^{2+}, sulfate	pH: 3.5–6 Pb^{2+}:1×10^{-3} M Sulfate: $3 \times 10^{-5} - 4.5 \times 10^{-3}$ M	ATR-FTIR and EXAFS	Formation of ternary surface complexes and electrostatic effects	Elzinga et al., 2001
Goethite, Cu^{2+}, sulfate	pH: 2–13 Cu^{2+}: 0.94 and 1.04 mM Sulfate: 0.21–1.04 M Goethite: 1 g L^{-1}	Batch experiments and Zeta Potential measurement	Electrostatic effects	Juang and Wu, 2002
Goethite/γ-Al_2O_3/bayerite, Hg^{2+}, sulfate	pH: 4–8 Hg^{2+}: 0.5 mM Sulfate: $10^{-5} - 0.9$ M Goethite/γ-Al_2O_3/bayerite: 10 g L^{-1}	EXAFS	Formation of ternary surface complexes	Kim et al., 2004
Goethite, Cd^{2+}, sulfate	pH: 4–8 Cd^{2+}: 0–0.5 mM Sulfate: 0.025–1 mM Goethite: 20 g L^{-1}	ATR-FTIR	Formation of Cd–SO_4 ternary surface complexes and electrostatic effects	Zhang and Peak, 2007
Goethite, Cu^{2+}, sulfate	pH: 3.5–9 Cu^{2+}: 0.1 mM Sulfate: $5 \times 10^{-7} - 1 \times 10^{-4}$ M Goethite: 0.1 g L^{-1}	ATR-FTIR and SCM	Electrostatic effects	Beattie et al., 2008
Hematite/goethite, Fe^{2+}, sulfate	pH: 3–9 Fe^{2+}: 0.1 and 1.0 mM Sulfate: 0.1 and 1.0 mM Hematite/goethite: 4 g L^{-1}	ATR-FTIR and SCM model	Formation of ternary complexes and electrostatic interactions	Hinkle et al., 2015

Abbreviations

ATR-FTIR: attenuated total reflectance Fourier transform infrared spectroscopy;
EXAFS: extended X-ray absorption fine structure spectroscopy;
SCM: surface complexation model.

co-sorbed SO_4^{2-} enhancing Cd^{2+}, Cu^{2+}, Pb^{2+}, and Zn^{2+} adsorption on goethite (Benjamin and Leckie, 1982).

Metal cations and sulfate can also form ternary complexes on mineral surfaces, as indicated by SCM and spectroscopic analyses (Table 3). Calculations via the TLM model indicated that the formation of ternary surface complexes between reactive surface sites, heavy metals, and sulfate must be included to reconcile the observed and predicted effects (Hoins, 1993). Sorption curves of Cu^{2+} and SO_4^{2-} in binary-sorbate systems were described with the generalized two-layer model (GTLM), assuming the formation of a Cu^{2+}–SO_4^{2-} ternary surface complex (Ali and Dzombak, 1996b). Cation-bridged ternary complexes were reported in the following co-sorption systems: Cu^{2+}–Zn^{2+} and Co^{2+}/Pb^{2+}/Cd^{2+}–SO_4^{2-} on ferrihydrite (Swedlund and Webster, 2001; Swedlund et al., 2003), and Cu^{2+}/Pb^{2+}/Cd^{2+}/Zn^{2+}–SO_4^{2-} on goethite (Swedlund et al., 2009; Ostergren et al., 2000a). ATR-FTIR spectra showed that the cooperative adsorption of aqueous Fe(II) and sulfate likely resulted from a combination of ternary complexation and electrostatic interactions. SCM calculations must include ternary complexes to simulate all conditions corresponding to the macroscopic data, further implying that Fe(II) and sulfate formed ternary complexes on iron (oxyhydr)oxide surfaces (Hinkle et al., 2015).

The dominant mechanisms that contribute to metal–sulfate co-adsorption are dependent on solution pH and the concentrations of metal ions and sulfate (Table 3). For example, ATR-FTIR and EXAFS analyses indicated the formation of Cd^{2+}–SO_4^{2-} and Pb–SO_4^{2-} ternary surface complexes on goethite and that electrostatic effects also contributed to their co-sorption (Fig. 6). The relative importance of ternary complex formation vs. electrostatic effects in the co-sorption system depended on solution pH values and Cd^{2+}/Pb^{2+} concentrations. The formation of ternary complexes was dominant at low pH values and high Cd^{2+}/Pb^{2+} concentrations, whereas electrostatic effects were more pronounced at high pH values and low Cd^{2+}/Pb^{2+} concentrations. A fraction of the SO_4^{2-} ions, which initially sorbed as inner-sphere complexes on goethite in the absence of Cd^{2+}/Pb^{2+}, transformed into Cd^{2+}/Pb^{2+}–SO_4^{2-} ternary complexes with increasing Cd^{2+}/Pb^{2+} concentration (Elzinga et al., 2001; Zhang and Peak, 2007). Additionally, the presence of sulfate enhanced Hg(II) adsorption on goethite through electrostatic interactions. EXAFS analysis indicated that

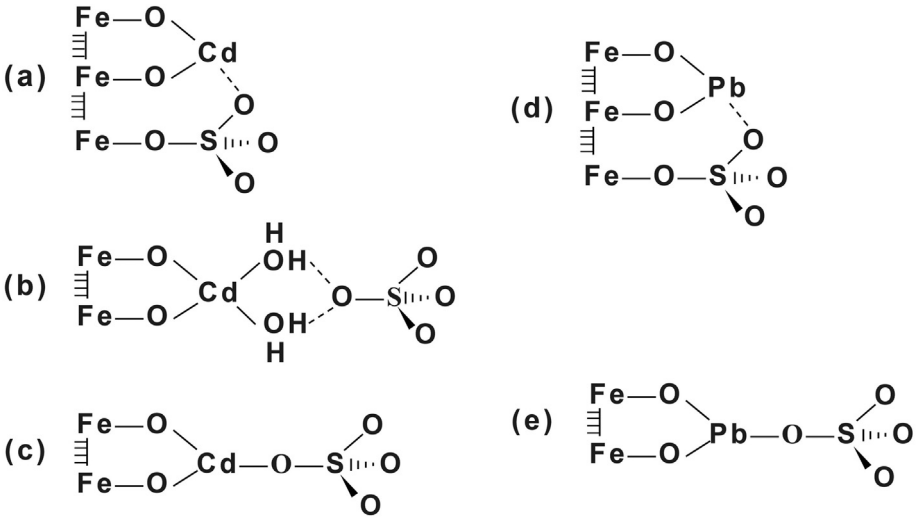

Fig. 6. Proposed configurations of cadmium (Cd) and sulfate ternary complexes (configuration a, b, and c), modified from Zhang and Peak (2007); and lead (Pb) and sulfate ternary complexes (configuration d and e) on goethite, modified from Elzinga et al. (2001). Different complexation configurations can co-exist within the same system.

Table 4
Interaction mechanisms of metal ion and organic ligands co-sorption on various minerals.

Systems	Reaction conditions	Methodology	Co-sorption mechanisms	Reference
Goethite, Cd^{2+}, oxalate	pH: 5.31 Cd^{2+}: 403 ppm Oxalate: 1.8 mM Goethite: 18 g L^{-1}	EXAFS	Formation of cadmium oxalate precipitates	Collins et al., 1999
Goethite, Cu^{2+}, oxalate	pH: 2–9 Cu^{2+}: 5×10^{-6} M Oxalate: 0.5 mM Hematite: 0.5 g L^{-1}	DLM	Formation of type A ternary complex	Buerge-Weirich et al., 2003
Hematite nanoparticles and microparticles, Zn^{2+}, oxalate	pH: 5.5 Zn^{2+}: 0.8–7.5 mM Oxalate: 8 mM Hematite: 10 g L^{-1}	ATR-FTIR and EXAFS	Formation of inner-sphere oxalate, outer-sphere $Zn–oxalate_{(aq)}$, and/or type A ternary complexes on hematite microparticles; Formation of inner-sphere oxalate, outer-sphere Zn-oxalate $complexes_{(aq)}$, Zn-oxalate-like surface precipitates and type B ternary surface complexes on hematite nanoparticles.	Ha et al., 2009
Hematite, Ni^{2+}, oxalate	pH: 7 Ni^{2+}: 0–1 mM Oxalate: 0.1 and 1 mM Hematite: 1 g L^{-1}	EXAFS and ATR-FTIR	Formation of ternary surface complexes	Flynn and Catalano, 2017
α-Al_2O_3, Cd^{2+}, citrate	pH: 3–10 Cd^{2+}: 0.1 mM Citrate: 0.1 and 1 mM α-Al_2O_3: 100 g L^{-1}	SCM	Formation of ternary surface complexes at low pH and aqueous Cd–citrate complexation at high pH (>7.2)	Boily and Fein, 1996
Goethite, Cd^{2+}, citrate	pH: 5.36 Cd^{2+}: 403 ppm Citrate: 1.8 mM Goethite: 18 g L^{-1}	EXAFS	Formation of cadmium citrate precipitates	Collins et al., 1999
Goethite, Cd^{2+}, citrate	pH: 3–10 Cd^{2+}: 0.05 mM Citrate: 0.05–1 mM Goethite: 2 g L^{-1}	ATR-FTIR and Surface complexation model	Formation of ternary surface complexes	Lackovic et al., 2004
Kaolinite, Zn^{2+}, citrate	pH: 4.5–7.5 Zn^{2+}: 1.5 mM Citrate: 1.5 mM Kaolinite: 20 g L^{-1}	EXAFS	Formation of Zn—Al LDH surface precipitates in the absence of citrate and outer-sphere complexes in the presence of citrate	Stietiya et al., 2011
γ-Al_2O_3, Zn^{2+}, citrate	pH: 6.5 Zn^{2+}: 1 mM Citrate: 0–2 mM γ-Al_2O_3: 1 g L^{-1}	Batch experiments	Formation of aqueous Zn–citrate complexes	Stietiya and Wang, 2014
γ-Al_2O_3, Cu^{2+}, glutamate	pH: 4–9 Cu^{2+}: 0.5 mM Glutamate: 1.5 mM γ-Al_2O_3: 2 g L^{-1}	EXAFS and FTIR	Formation of type B complexes at acid pHs and type A complexes at alkaline pHs	Fitts et al., 1999
Hematite, Pb^{2+}, malonic acid	pH: 4–8 Pb^{2+}: 0.06 and 0.1 mM Malonic acid: 0.1 and 0.6 mM Hematite: 0.2 and 1 g L^{-1}	EXAFS and ATR-FTIR	Formation of ternary surface complexes	Lenhart et al., 2001
γ-Al_2O_3, Cd^{2+}, poly(acrylic acid)	pH: 4–10 Cd^{2+}: 10^{-5} M poly(acrylic acid): 0.049–0.23 g L^{-1} γ-Al_2O_3: 2 g L^{-1}	DLM	Formation of ternary surface complexes at pH < 6 and soluble Cd–poly(acrylic acid) complexes at pH > 6	Floroiu et al., 2001
Goethite, Cd^{2+}, phthalate	pH: 3.5–9.5 Cd^{2+}: 0.04–0.4 mM Phthalate: 1.4–11.4 mM Goethite: 2 and 4 g L^{-1}	EXAFS, FTIR, and SCM	Formation of ternary inner-sphere complexes	Boily et al., 2005
Rutile, Ca^{2+}, lysine	pH: 3–11 Ca^{2+}: 1 and 3 mM Lysine: 10 μM Rutile: 3 g L^{-1}	SCM	Electrostatic effects	Lee et al., 2014
Montmorillonite, Ca^{2+}, lysine	pH: 4–10 Ca^{2+}: 1 mM Lysine: 1–10 mM Montmorillonite: 10 g L^{-1}	ATR-FTIR	Electrostatic effects	Yang et al., 2016
Brucite, Ca^{2+}, lysine	pH: 10.2 Ca^{2+}: 4.1 mM Lysine: 10–150 μM Brucite: 1 g L^{-1}	SCM	Electrostatic effects	Estrada et al., 2019
Goethite, Cu^{2+}, PMG [*N*-(phosphonomethyl) glycine]	pH: 3–9 Cu^{2+}: 1.87 mM PMG: 1.87 mM Goethite: 10 g L^{-1}	ATR-FTIR and EXAFS	Formation of B-type ternary surface complexes at pH 4 and A-type ternary surface complexes at pH > 4	Sheals et al., 2003
Manganite, Cd^{2+}, PMG	pH: 6–10 Cd^{2+}: 2 and 3 mM PMG: 2 and 3 mM Manganite: 5 and 10 g L^{-1}	FTIR and EXAFS	Formation of B-type ternary complexes	Ramstedt et al., 2005
γ-Alumina, Zn^{2+}, PMG	pH: 5.5 and 8 Zn^{2+}: 0–1 mM PMG: 1 mM γ-alumina: 4 g L^{-1}	^{31}P NMR and EXAFS	Formation of γ-alumina-PMG-Zn ternary surface complexes	Li et al., 2013b
Hematite, Cd^{2+}, phytate	pH: 4–10 Zn^{2+}: 0–0.2 mM Phytate: 0.03 mM Hematite: 0.7 g L^{-1}	ATR-FTIR	Formation of two structurally distinct ternary surface complexes	Wan et al., 2017
γ-Al_2O_3, Zn^{2+}, phytate	pH: 4–7 Zn^{2+}: 0.24–3.0 mM Phytate: 0.24 mM γ-Al_2O_3: 0.75 g L^{-1}	NMR and EXAFS	Formation of ternary surface complexes and zinc–phytate precipitates	Yan et al., 2018a
Goethite, Zn^{2+}, phytate	pH: 3–10 Zn^{2+}: 0–0.5 mM Phytate: 0.03 mM goethite: 0.5 g L^{-1}	ATR-FTIR	Formation of type B ternary surface complexes	Yan et al., 2018b
Montmorillonite/kaolinite, Cu^{2+}/Zn^{2+}/Cd^{2+}, DFOB	pH: 4–10 Cu^{2+}/Zn^{2+}/Cd^{2+}: 0.01–0.085 mM DFOB: 0.3 mM Montmorillonite/kaolinite: 1 g L^{-1}	SCM	Electrostatic effects	Neubauer et al., 2000
γ-Al_2O_3, rare-earth elements, DFOB	pH: 7.1 Rare-earth elements: 1 mg L^{-1} DFOB: 0.5 mM γ-Al_2O_3: 2 g L^{-1}	XANES	DFOB promotes rare-earth element adsorption, and the promotive effect reduces as the atomic number increases	Yoshida et al., 2004

Abbreviations

AFM: atomic force microscopy;
ATR-FTIR: attenuated total reflectance Fourier transform infrared spectroscopy;
CD-MUSIC: charge distribution multi-site complexation;
DFT: density functional theory;
DLM: diffuse layer model;
EXAFS: extended X-ray absorption fine structure spectroscopy;
NMR: nuclear magnetic resonance spectroscopy;
SCM: surface complexation model;
XANES: X-ray absorption near edge structure spectroscopy;
XPS: X-ray photoelectron spectroscopy.

when the concentration of SO_4^{2-} increased from 0.1 M to 0.93 M, the Hg—Fe coordination distance noticeably increased from 3.26 Å to 3.70 Å, suggesting the formation of ternary surface complexes in the Hg–goethite–sulfate system at high SO_4^{2-}concentration (Kim et al., 2004).

Surface precipitation possibly occurs in some metal–sulfate co-sorption systems. For example, the presence of sulfate was found to enhance the ability of boehmite and goethite to adsorb Pb^{2+}. In the presence of Pb^{2+}, free sulfate ions were more effectively adsorbed on boehmite as the Pb^{2+} concentration increased. EXAFS analysis suggested the formation of lead sulfate precipitates at the surface of goethite (Weesner and Bleam, 1998).

Overall, compared with phosphate and arsenate which show strong affinity to mineral surfaces (e.g., iron and aluminum (oxyhydr)oxides), sulfate has a relatively weak affinity. Generally, sulfate sorbs on minerals via outer- and inner-sphere complexes (Elzinga et al., 2001; Zhang and Peak, 2007; Beattie et al., 2008). The cooperative adsorption of sulfate with metal ions is promoted mainly by ternary complexation and electrostatic interactions. However, these effects are weak compared to systems where phosphate and arsenate are added. Therefore, the remediation of heavy metal-contaminated environments using sulfate is not promising since the formed products are unstable and the introduction of excess sulfate may result in sulfate pollution and sulfide production with the associated toxicity (Lamers et al., 1998).

3. Co-sorption of metal ions and organic ligands on minerals

Low-molecular-weight organic ligands are ubiquitous in natural environments and can interact with metal cations during co-sorption on mineral surfaces because of their negative charge (Collins et al., 1999; Stietiya et al., 2011; Zhang et al., 2019). Herein, we mainly focus on low-molecular-weight organic acids (e.g., oxalate, citrate, and phthalate), amino acids, PMG, IHP, and the siderophore desferrioxamine B (DFOB), which are most commonly observed in the environments. The presence of organic ligands generally increases the sorption of metal ions on minerals via the formation of ternary surface complexes or surface precipitates, but can also inhibit the sorption of metal ions due to the formation of aqueous complexes. The type of interaction (promotive vs competitive) is greatly dependent on identity and properties of minerals, species and concentrations of metal ions and organic ligands, and solution pH.

3.1. Co-sorption of metals with low-molecular-weight organic acids

3.1.1. Co-sorption of metals with oxalate

Ternary metal-ligand surface complexation and surface precipitation are the dominant mechanisms of metal–oxalate co-sorption on mineral surface (Table 4). For example, the presence of oxalate inhibited Ni^{2+} sorption on hematite and goethite, since oxalate complexed with aqueous Ni^{2+}, which decreased Ni(II) surface sorption density on minerals. EXAFS analyses indicated that in the presence of oxalate, the adsorbed Ni^{2+} coordinated to fewer Fe atoms on hematite surface, and the edge-sharing complexes owned a longer Ni–Fe interatomic distance. At pH 7, ATR-FTIR spectra of oxalate adsorbed onto hematite in the presence of Ni showed obvious differences to IR spectra of 10 mM aqueous oxalate and Ni–oxalate co-precipitate standard compounds. These changes in binding affinity/coordination were attributed to the formation of Ni–oxalate ternary surface complexes, as shown in Fig. 7 (Flynn and Catalano, 2017). Similarly, the presence of oxalate reduced Cu^{2+} adsorption on goethite at high pH values because of the competition between solution and surface complexation of Ni and oxalate. At pH < 6, Cu^{2+} adsorption curve could be best explained in terms of a type A ternary complex in the presence of oxalate (Buerge-Weirich et al., 2003). ATR-FTIR and EXAFS analyses pointed to the formation of ternary metal–oxalate surface complexes as one of the main coordination modes for the co-sorption of Al^{3+} or Ga^{3+} and oxalate on goethite (Simanova et al., 2011).

Surface precipitation is commonly observed in many metal and oxalate co-sorption systems. For example, Cd K-edge EXAFS analysis showed that the coordination environment of Cd co-sorbed with oxalate on goethite was similar to that of cadmium oxalate solid phase. The calculated saturation index of $CdC_2O_4 \cdot 3H_2O$, log (IAP (Ion-activity product) / K_{sp}) = 1.45 indicated that this co-sorption system was supersaturated with respect to Cd-oxalate precipitates. Thus, enhanced sorption of Cd^{2+} on goethite in the presence of oxalate could be attributed to the formation of cadmium oxalate surface precipitates (Collins et al., 1999).

Mineral particle size and metal/oxalate ratio are considered as main parameters that influence the co-sorption mechanism. For example, the sorption of Zn^{2+} onto hematite nanoparticles (HNs) and hematite microparticles (HMs) in the presence of oxalate was studied as a function of Zn^{2+}/oxalate concentration ratios (R). In the Zn^{2+}/oxalate/HM ternary system, ATR-FTIR and EXAFS spectra at R values of 0.16 and 0.68 indicated the presence of inner-sphere oxalate, outer-sphere Zn–oxalate$_{(aq)}$, and/or type A ternary complexes (i.e., ≡O_2–Zn–oxalate). Both inner-sphere oxalate and outer-sphere Zn-oxalate$_{(aq)}$ complexes were also formed in the Zn^{2+}/oxalate/HN ternary system at R = 0.15. In contrast, ATR-FTIR and EXAFS spectra of Zn^{2+}/oxalate/HN sample at R = 0.68 indicated the formation of Zn-oxalate$_{(s)}$-like surface precipitates and possibly type B ternary surface complexes (i.e., ≡O_2-oxalate-Zn) (Ha et al., 2009).

3.1.2. Co-sorption of metals with citrate

Co-sorption characteristics of metal ions and citrate on minerals are dependent on solution pH, mineral properties, and citrate concentration. Citrate exerted opposing effects on metal (such as Cd^{2+} and

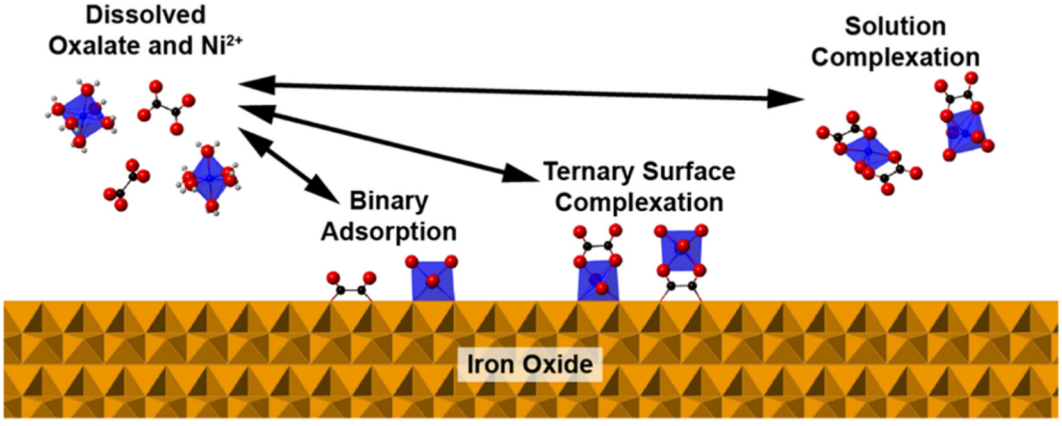

Fig. 7. Schematic diagram of co-sorption mechanisms of nickel ion (Ni^{2+}) and oxalate on iron (oxyhydr)oxides (hematite and goethite) (Flynn and Catalano, 2017). Red, black, and white spheres denote oxygen, carbon, and hydrogen atoms, respectively. Blue octahedrons denote hydrated nickel ions. (For interpretation of the references to colour in this figure legend, the reader is referred to the web version of this article.)

Zn^{2+}) adsorption. For example, the presence of citrate enhanced Cd^{2+} adsorption on α-Al_2O_3 between pH 3.5 and 7.2, but inhibited it at pH > 7.2 (Boily and Fein, 1996). Similarly, citrate slightly increased the extent of Zn^{2+} adsorption on kaolinite at pH < 5.7, but greatly inhibited it at pH > 5.7 (Stietiya et al., 2011). In the absence of citrate, montmorillonite showed a higher Ni^{2+} sorption ability than goethite. However, in the presence of 100 μM citrate, goethite became a stronger Ni^{2+} adsorbent than montmorillonite, because citrate greatly decreased Ni^{2+} sorption on montmorillonite (Marcussen et al., 2009). The adsorption of Cd^{2+} and Pb^{2+} on goethite and montmorillonite was facilitated by citrate at low concentrations (<0.6–1.0 mM), but was inhibited at 1.0–3.0 mM concentrations. The inhibitive effect was much stronger on Pb^{2+} than Cd^{2+} adsorption. Meanwhile, the effect of the citrate loadings on Cd^{2+} and Pb^{2+} adsorption was stronger on goethite than on montmorillonite (Huang et al., 2010). Due to the presence of permanent negative charges in montmorillonite, citrate addition has less impacts on metal ion adsorption on montmorillonite when compared with goethite (with positive surface charge).

Ternary surface complexation is one of the main adsorption mechanisms for promotive citrate–metal co-sorption. Lackovic et al. (2004) found that the formation of ternary Cd(II)–citrate surface complexes led to an increase in the extent of Cd^{2+} sorption on goethite at pH > 4. In another study, the formation of ternary surface complexes (≡Al-Citrate-Cd) enhanced Cd^{2+} adsorption on α-Al_2O_3 surface at low pH values (3.5–7.2), but citrate reduced the extent of Cd^{2+} adsorption at alkaline pHs (>7.2) due to the formation of aqueous metal–citrate complexes (Boily and Fein, 1996). Nano-particulate hydrated zirconium oxide (ZrO_2) confined inside the anion exchanger D201 (nanocomposite HZO-201) displayed an excellent adsorption capacity for Cu(II)–citrate (~130 mg Cu/g Zr), even under high salinity conditions. Scanning transmission electron microscopy coupled with X-ray energy-dispersive spectroscopy (STEM-EDS), ATR-FTIR, and XPS analyses indicated that the formation of a ternary complex of Cu(II), citrate, and the embedded nano-HZO promoted the removal of Cu(II)–citrate by HZO-201 (Zhang et al., 2019).

At the same time, the presence of citrate can prevent surface precipitation of metal ions (e.g., Zn^{2+}, Ni^{2+}, and Cd^{2+}) on Al-bearing minerals (e.g., gibbsite and kaolinite) through aqueous metal–citrate complexation (Table 4). For example, in the absence of organic ligands, a large amount of Ni^{2+} was taken up by gibbsite and pyrophyllite via the formation of Ni—Al LDH precipitates. However, citrate formed dissolved complexes with Ni^{2+}, leading to reduced concentration of free Ni^{2+} and decreased formation of Ni-related surface precipitates. In the presence of citrate, the surface precipitate's phase was Ni—Al LDH on pyrophyllite, but predominately α-Ni hydroxide on gibbsite (Yamaguchi et al., 2001). The inhibitive effect of citrate on Ni^{2+} sorption was greater on gibbsite due to its small surface area (Yamaguchi et al., 2002). Zn K-edge EXAFS analysis pointed out that Zn^{2+} ions adsorbed on kaolinite formed Zn—Al LDH surface precipitates in the absence of citrate and outer-sphere complexes in the presence of citrate (Stietiya et al., 2011). The presence of citrate reduced Zn^{2+} adsorption but increased Cd^{2+} adsorption on Al oxide nanoparticles when compared to the Zn– or Cd–mineral binary systems. These effects could be attributed to the weak adsorption of citrate to Al oxide nanoparticles and the formation of various aqueous citrate–Zn complexes, which prevented Zn^{2+} from binding to the surface of Al oxides (Stietiya and Wang, 2014).

Al-bearing minerals (e.g., gibbsite, pyrophyllite and kaolinite) can be considered as promising candidates to remediate Zn-or Ni-contaminated field sites via the immobilization of Zn^{2+} and Ni^{2+} as Zn- or Ni—Al LDH precipitates. However, the presence of organic ligands (e.g., citrate) may increase the mobility, availability and phytotoxicity of heavy metals due to the formation of aqueous citrate–metal complexes, which should be considered for the remediation of such metal contaminants.

3.1.3. Co-sorption of metals with phthalate

Phthalate and phthalic acid esters are ubiquitous in the environment, because of their widespread application in the manufacture and processing of plastic products as plasticizers. (Net et al., 2015). Spectroscopic and modeling analyses have been applied to reveal co-sorption mechanisms of metal ions and phthalate on minerals. The presence of phthalate enhanced Cu^{2+} sorption on goethite at low pH values (pH < 5.5). The sorption of Cu^{2+} could be quantitatively simulated by the GTLM which included a unique set of Cu^{2+}–phthalate ternary surface complexes for different conditions (e.g., pH and Cu/phthalate concentration ratio) (Ali and Dzombak, 1996a). According to the DLM, the presence of phthalate resulted in both promotive (due to the formation of ternary surface complexes) and competitive (due to the formation of aqueous complexes in solution) effects on Cu^{2+} and Cd^{2+} sorption on ferrihydrite, depending on the reaction conditions (Song et al., 2008, 2009). Additionally, based on EXAFS, FTIR, and SCM analyses, ternary inner-sphere complexation of phthalate with Cd^{2+} being coordinated via either an inner-sphere (at pH 3.5–9.5) or outer-sphere (only present at pH > 6) phthalate complex were also proposed to explain the behavior of Cd^{2+} and phthalate co-sorption on goethite surfaces (Boily et al., 2005).

3.1.4. Co-sorption of metals with other common organic acids

Other common organic acids with low molecular weight, such as benzene carboxylic acids, tartrate, malonic acid, salicylate, and pyromellitate, are also widely found in natural environments. The properties of minerals, species and concentration of organic acids, solution pH, and addition sequence of organic acids and metal ions have been reported to regulate the co-sorption behavior of these organic ligands and metals on environmentally relevant minerals (Angove and Wells, 1999; Floroiu et al., 2001; Violante et al., 2003). Angove and Wells (1999) investigated the influence of different benzene carboxylic acids (phthalic, hemimellitic, trimellitic, trimesic, pyromellitic, and mellitic acids) on Cd^{2+} sorption to goethite and kaolinite. At 10^{-3} M concentrations, all acids enhanced Cd^{2+} adsorption on goethite, with the higher members of the series (i.e., benzene carboxylic acids with higher number of carboxyl) being the most effective. These members also inhibited Cd^{2+} adsorption onto kaolinite, although the phthalic and trimesic acids produced a slightly increased extent of adsorption. Violante et al. (2003) studied the sorption of Pb^{2+} on Fe, Al, and Fe—Al oxides in the absence and presence of tartrate and designed experiments considering the effects of metal and tartrate addition sequence (such as addition of Pb^{2+} alone, addition of a tartrate/Pb^{2+} mixture, Pb^{2+} addition before tartrate, and Pb^{2+} addition after tartrate). For the three oxide minerals studied, the largest amounts of sorbed Pb were observed when tartrate was added before Pb^{2+}, and Pb^{2+} adsorption densities followed the order: tartrate before Pb^{2+} > Pb^{2+} before tartrate > Pb^{2+} + tartrate together > Pb^{2+} alone. The addition sequence therefore played an important yet underappreciated role in interpreting results of laboratory experiments.

The formation of ternary surface complexes is considered as the main mechanism for metal–organic acid co-sorption. Type A metal-bridging surface complexes formed in hematite–Pb^{2+}–malonic acid and goethite–Cu^{2+}–salicylate systems at pH > 5 (Lenhart et al., 2001; Buerge-Weirich et al., 2003). The formation of type B ternary surface complexes was proposed as an active mechanism for goethite–pyromellitate–Cu^{2+}/Cd^{2+} and goethite/kaolinite–benzene carboxylic acids–Cd^{2+} co-sorption at acidic pH (Angove and Wells, 1999; Buerge-Weirich et al., 2003). The presence of poly(acrylic acid) promoted Cd^{2+} adsorption on γ-Al_2O_3 below pH 6 mainly via ternary surface complexes. However, the extent of Cd^{2+} adsorption decreased above pH 6 since the formation of aqueous Cd–poly(acrylic acid) complexes competed with surface-adsorbed Cd^{2+} (Floroiu et al., 2001).

3.2. Co-sorption of metals with amino acids

Biomolecules such as amino acids are ubiquitous in soils, sediments, and natural waters. The interactions between minerals and amino acids are of fundamental interest in a variety of environmental or geological

processes, such as biomineralization, biomedicine, short- and long-term carbon cycles, and the chemical evolution of life on Earth (Lee et al., 2014; Yang et al., 2016). The adsorption of amino acids on minerals plays an essential role for the mobility, bioavailability, and degradation of amino acids in the environment (Yang et al., 2016). The co-existence of amino acids and metal ions mutually affects their interfacial reactions on minerals.

In the presence of chelidamic acid, Cu^{2+} sorption on goethite considerably increased at pH < 5. In contrast, Ca^{2+} sorption decreased in the presence of chelidamic acid, especially at high pH, due to the formation of aqueous Ca^{2+}–chelidamic acid complexes in solution (Ali and Dzombak, 1996a). The formation of aqueous Ca^{2+}-amino acid complexes also dramatically reduced the adsorption capacity of lysine on rutile, montmorillonite, and brucite, due to electrostatic effects (Lee et al., 2014; Yang et al., 2016; Estrada et al., 2019).

Amino acids affect metal sorption on natural minerals mainly via the formation of ternary surface complexes. The sorption of Cu^{2+} in the presence of chelidamic acid could be quantitatively simulated at pH 3–6.5 by the GTLM which included ternary surface complexation (Ali and Dzombak, 1996a). Similarly, in the presence of glycine, adsorption of Cu^{2+} on gibbsite and boehmite led to the formation of a ternary complex, whose structure involved metal coordination with a surface hydroxyl and at least one glycine molecule (McBride, 1985). EXAFS and FTIR analyses indicated that two typical complexes were primarily responsible for Cu^{2+} and glutamate co-sorption on γ-Al_2O_3 at pH 4–9. Under acidic conditions, glutamate served as a bridge to connect Cu^{2+} and the (hydr)oxide surface as type B complexes. Under alkaline conditions, the relative amount of surface-bound Cu(II) complexes increased and the formation of type A complexes (with Cu(II) bridging between glutamate and mineral surface) became the dominant mechanism to explain the promotive adsorption of glutamate and Ca^{2+} on γ-Al_2O_3 (Fitts et al., 1999).

3.3. Co-sorption of metals with PMG

PMG (*N*-(phosphonomethyl)glycine or glyphosate), as the most extensively used herbicide in agricultural production worldwide, is widely detected in the environment (Hébert et al., 2019). Like previously discussed anions and organic ligands, the presence of PMG can affect the sorption of metal ions on environmental minerals via promotive or competitive effects. For example, when the solution pH was below 5, the presence of PMG increased the amount of Zn^{2+} sorbed on goethite, because Zn^{2+} was adsorbed on the surface with PMG acting as a bridge. In contrast, at pH > 5, the presence of PMG reduced the adsorption amounts of Zn^{2+} on goethite since PMG chelated with aqueous Zn^{2+} to form water-soluble complexes, which had lower affinity for the goethite surface than Zn^{2+} alone (Wang et al., 2008). PMG adsorption density on montmorillonite decreased in the presence of Cu^{2+}, owing to the lower adsorption tendency of the formed aqueous Cu–PMG complexes on montmorillonite when compared to that of free PMG (Morillo et al., 1997). However, the presence of Cd^{2+} led to an increased PMG adsorption on the manganite surface over a wide pH range, compared to the corresponding PMG–mineral binary system (Ramstedt et al., 2005).

The formation of ternary complexes is one of the main mechanisms affecting metal–PMG co-sorption (Table 4). For example, Cd(II) and PMG formed type B ternary surface complexes on manganite (Ramstedt et al., 2005). Cu^{2+} and PMG could form type B ternary surface complexes on goethite at pH 4, whereas type A ternary surface complexes were observed at pH > 4 (Sheals et al., 2003). In the presence of PMG, ^{31}P NMR and EXAFS studies showed the formation of γ-alumina-PMG-Zn ternary surface complexes, in which PMG was bound to γ-alumina surface via a phosphonate group that acted as a bridge between mineral surface and Zn^{2+}. The addition sequence of PMG and Zn^{2+} remarkably influenced their co-sorption behaviors and mechanisms on γ-alumina. At pH 8, Zn—Al LDH precipitates formed when Zn^{2+} was added first, whereas no precipitation occurred when PMG was added first or simultaneously with Zn^{2+}. In contrast, at pH 5.5, only γ-alumina–PMG–Zn ternary surface complexes were formed, regardless of the addition sequence of PMG and Zn^{2+} (Li et al., 2013b).

3.4. Co-sorption of metals with IHP

Myo-inositol hexaphosphate (IHP) is a common organic phosphate widely found in soil environments (Turner et al., 2002). Ternary surface complexation and precipitation are the two main mechanisms proposed to explain metal and IHP co-sorption on natural minerals (Table 4). For example, in a hematite–IHP–Cd ternary system, the presence of aqueous Cd^{2+} enhanced IHP sorption relative to that in a binary hematite–IHP system. This enhancement was more pronounced as solution pH increased, in contrast to the pH-dependence of IHP sorption in the binary system. Also, the simultaneous presence of IHP promoted the retention of Cd^{2+} on hematite, and two structurally distinct ternary surface complexes were proposed to explain the co-sorption of Cd^{2+} and IHP on hematite (Wan et al., 2017). The formation of goethite–IHP–Zn ternary surface complexes was the most likely mechanism for promotive co-adsorption of IHP and Zn^{2+} on goethite, indicated by in-situ ATR-FTIR differentiation analysis (Yan et al., 2018b).

The presence of IHP significantly increased Cd^{2+} sorption on gibbsite below pH 8, especially at high concentrations of Cd^{2+} and IHP. Based on ^{31}P NMR spectra and SCM simulations, two outer-sphere ternary complexes were proposed to form on gibbsite in the co-presence of IHP and Cd^{2+} (Ruyter-Hooley et al., 2016). IHP strongly increased the amount of Cd^{2+} sorbed on kaolinite at pH 4–8. IHP was bound to the surface in both inner- and outer-sphere complexes, while two additional ternary complexes were required to fit the IHP–Cd(II)–kaolinite co-sorption via extended constant capacitance models. The inhibition of Cd^{2+} adsorption at high pH (>9) likely resulted from the formation of dissolved Cd(II)–IHP complexes (Ruyter-Hooley et al., 2017). The pre-sorbed IHP increased the sorption density of Zn^{2+} on γ-Al_2O_3 surfaces and prevented the formation of Zn—Al LDH precipitates, by increasing Zn^{2+} critical concentration required to precipitate surface Zn (II) complexes into Zn—Al LDH phase. NMR and EXAFS analyses further revealed that the chemical environment and speciation of pre-sorbed IHP changed (i.e., from inner-sphere to ternary surface complexes and zinc phytate precipitates) with increasing Zn^{2+} concentrations or pH (Yan et al., 2018a).

3.5. Co-sorption of metals with DFOB

Siderophores such as DFOB are small organic molecules produced from microorganisms under iron-limiting conditions, which function to improve iron uptake by the microorganisms. These compounds can chelate with divalent heavy metal ions and thus affect the transport and mobility of metals in the environments (Neubauer et al., 2000; Shirvani et al., 2006; Ahmed and Holmström, 2014; Saha et al., 2016; Karimzadeh et al., 2017).

Generally, DFOB displays two different roles that can increase or decrease metal sorption on environmental minerals (Stietiya et al., 2011; Karimzadeh et al., 2013; Hamidpour et al., 2019). Solution/environment pH can significantly determine the co-sorption mechanism of metal ions and DFOB on minerals. For example, at weakly acidic to neutral pH, the presence of DFOB increased the amount of heavy metals sorbed on zeolites due to the stronger sorption of positively charged metal–DFOB complexes. As solution pH increases (especially when pH values are higher than 7), DFOB affected Pb^{2+}, Zn^{2+}, and Cd^{2+} immobilization, and drastically inhibited (~80%) Zn sorption on mineral surfaces (Karimzadeh et al., 2013). It was also shown that the presence of DFOB slightly increased Zn^{2+} adsorption on kaolinite at pH ~5.7 or less, but greatly reduced it at pH > 5.7 (Stietiya et al., 2011). In the presence of DFOB, the adsorption of Cd^{2+} and Zn^{2+} onto muscovite and

phlogopite was reduced particularly from neutral to alkaline pH (Hamidpour et al., 2019), whereas DFOB strongly reduced Eu^{3+} adsorption on goethite and boehmite at pH > 6 (Kraemer et al., 2002). At pH 4, DFOB did not appreciably bind with aqueous Pb^{2+}, and its presence has limited impacts on Pb^{2+} adsorption behavior. However, at pH 6, DFOB slightly enhanced Pb adsorption, due (at least in part) to the formation of type A ternary surface complexes (DFOB–Pb–kaolinite). At pH 7.5, the presence of DFOB reduced Pb^{2+} sorption. Type A ternary complexes were the dominant surface species on kaolinite as indicated by EXAFS analysis (Mishra et al., 2010).

Additionally, the properties of minerals and species of metal ions can regulate co-sorption characteristics of metals and DFOB (Table 4). The sorption of Cu^{2+}, Zn^{2+}, and Cd^{2+} on montmorillonite was enhanced by the presence of DFOB through electrostatic interactions, and inhibitive effects of DFOB on Zn^{2+} and Cd^{2+} sequestrations were observed only at relative high pH values. However, DFOB significantly reduced heavy metal sorption on kaolinite (at pH 7–10). The different effects of DFOB on metal sorption by montmorillonite and kaolinite were due to the difference in permanent negative surface charge of these two minerals, responsible for the sorption of positively charged metal–DFOB complexes (Neubauer et al., 2000). In the ferrihydrite suspension, the presence of DFOB completely prevented Cu^{2+} sorption within a pH range of pH 4–10. A strong mobilizing effect was observed for Zn^{2+} adsorption, but not for Cd^{2+}. In the goethite system, enhanced sorption of Cu^{2+}, Zn^{2+}, and Cd^{2+} was observed in the presence of DFOB only at pH below 5, 7, and 8, respectively (Neubauer et al., 2002). Meanwhile, in the presence of DFOB, the adsorption of rare-earth elements on γ-Al_2O_3 tended to decrease at neutral pH as their atomic number increased (Yoshida et al., 2004).

4. Conclusions and perspectives

To explore how environmental factors affect the mobility of metal cations and naturally occurring anions/ligands in the environments, many macroscopic and spectroscopic studies combined with quantum chemical and SCM simulations have been conducted in the past three decades. The mechanism of metal–anion/ligand co-sorption depends on various geochemical conditions, such as mineral identity and properties (e.g., crystallinity and particle size), pH, species and concentrations of metal ions and anions/ligands, addition sequence of co-sorbed ions, and reaction time. The co-presence of metal ions and anions/ligands can affect each other's sorption behavior on mineral surfaces through promotive or competitive effects. Promotive effects are commonly attributed to surface electrostatic interactions, formation of ternary surface complexes, and surface precipitation. Competitive effects generally result from solution complexation or surface site competition.

The presence of inorganic anions has been shown to increase the sorption of metal ions on minerals. The co-sorption mechanisms are dependent on the species of inorganic anions. Particularly, co-sorption mechanisms of metal ion-phosphate/arsenate/selenite/silicate systems include surface electrostatic interactions, ternary surface complexation, and surface precipitation. Compared to the promotive effects of phosphate and arsenate on the retention of metal ions on minerals, the promotive effect by sulfate is relatively weak. Surface electrostatic effects and ternary surface complexation are the two dominant mechanisms for metal-sulfate co-sorption on mineral surface.

In addition, the concentrations of metal ions and inorganic anions remarkably affect the co-sorption mechanisms. Even at low concentrations, ternary surface complexes of metal-inorganic anions form on mineral surfaces. At very high concentrations, when the co-sorbed metal and inorganic anions in solution might be supersaturated with respect to their corresponding precipitates, bulk precipitation may occur. However, in some cases, even below the critical concentration of bulk precipitation for metals and inorganic anions, surface promotive co-sorption (via concentrating metal and anion contents at the mineral surface) can still lead to the formation of surface precipitation due to a local oversaturation of metals and anions. The effect of metal and inorganic anion concentration on co-sorption mechanisms differs from various inorganic anions.

Organic ligands such as oxalate, citrate, phthalate, PMG, and DFOB, often increase the sorption of metal ions on minerals at acidic pH via the formation of ternary surface complexes (or surface precipitates in some cases), but inhibit metal ion sorption on minerals due to the formation of aqueous metal-ligand complexes above neutral pH. The threshold pH of sorption promotion and inhibition differs from different organic ligands, depending on their chelating abilities that are related to their acid dissociation constants (pK_a) values. Organic ligands (e.g., citrate, oxalate and so on) are excellent candidates for the extraction of heavy metals (e.g., Cd, Cu, Pb, and Zn) from environmental particles (Gao et al., 2003; Shahid et al., 2012; Yang et al., 2020), which could significantly increase the mobility, availability and phytotoxicity of heavy metals. Organic ligands are thus not desirable for the remediation of heavy metal-contaminated soils/sites. However, organic ligands (e.g., oxalate and γ-polyglutamic acid) could be used to activate phosphate-containing rocks to increase dissolved phosphate contents in the amended soils, enhancing the immobilization of heavy metals by the released phosphate (Zhu et al., 2015).

Ternary surface complexation between metal ions and anions/ligands on mineral need to be considered in mechanistic models predicting the geochemical processes of metal ions in the environments. Appropriate parameters could be adopted for practical applications (e.g., remediation of sites contaminated by heavy metals and arsenate) based on the co-sorption characteristics and mechanisms of metal ions and inorganic anions/organic ligands. Despite substantial progress in understanding metal–anion/ligand co-sorption on minerals, the reaction features and molecular-level mechanisms of co-sorption under complex environmental conditions still need to be further explored. Based on the existing knowledge, future studies should primarily focus on the following aspects:

1) A variety of molecular-scale spectroscopic techniques combined with theoretical simulations, such as quantum chemical calculations and surface complexation modeling could be applied to understand the molecular reaction mechanisms and macroscopic co-sorption behavior of metals and anions/ligands on minerals. This will help to effectively predict environmental behavior of heavy metals and to control the associated contamination.
2) Future studies should explore the co-sorption of metal–anion/ligand on minerals under conditions closer to natural environments, which are mixed, complex, and multicomponent systems. For example, dissolved organic matter can strongly interact with iron oxides. In nature, ferric (oxyhydr)oxides such as ferrihydrite, abundant in soils and sediments, often associate with organic matter through forming mineral–organic aggregates via adsorption and/or co-precipitation (ThomasArrigo et al., 2017, 2018). The effects of coexisting dissolved organic matter (as surface coating or coprecipitate composition) on metal–anion/ligand co-sorption on minerals should be further investigated.
3) Changing anoxic or redox conditions widely occur in natural environments (Peiffer et al., 2021), such as contaminated coastal soils and paddy–upland rotation systems with the alternating flooding–drying conditions. The effects of redox fluctuations on metal–anion/ligand co-sorption on redox-sensitive minerals (especially iron and manganese oxides) should be considered in future research.
4) Finally, when phosphate-based or iron-based materials are applied for the remediation of heavy metal-contaminated soils, the potential secondary contaminations need to be strongly considered. Necessary strategies should be adopted to avoid possible secondary contaminations.

Declaration of competing interest

The authors declare no competing interests.

Acknowledgments

This research is supported by the National Key Research and Development Program of China (No. 2017YFD0200201), the National Natural Science Foundation of China (Grant Nos. 41603100 and 42030709), and the PhD Research Start-up Fund of Jiangxi Agricultural University (No. 050014-9232308146). AK acknowledges the infrastructural support by the DFG under Germany's Excellence Strategy, cluster of Excellence EXC2124, project ID 390838134.

References

Adebowale, K., Unuabonah, I., Olu-Owolabi, B., 2005. Adsorption of some heavy metal ions on sulfate- and phosphate-modified kaolin. Appl. Clay Sci. 29, 145–148.
Ahmed, E., Holmström, S.J.M., 2014. Siderophores in environmental research: roles and applications. Microb. Biotechnol. 7 (3), 196–208.
Ali, M.A., Dzombak, D.A., 1996a. Effects of simple organic acids on sorption of Cu2+ and Ca2+ on goethite. Geochim. Cosmochim. Acta 60 (2), 291–304.
Ali, M.A., Dzombak, D.A., 1996b. Interactions of copper, organic acids, and sulfate in goethite suspensions. Geochim. Cosmochim. Acta 60, 5045–5053.
Angove, M.J., Wells, J.D., 1999. Johnson BB. adsorption of cadmium(II) onto goethite and kaolinite in the presence of benzene carboxylic acids. Colloids Surf. A Physicochem. Eng. Asp. 146, 243–251.
Antelo, J., Arce, F., Fiol, S., 2015. Arsenate and phosphate adsorption on ferrihydrite nanoparticles. synergetic interaction with calcium ions. Chem. Geol. 410, 53–62.
Beattie, D.A., Chapelet, J.K., Gräfe, M., Skinner, W.M., Smith, E., 2008. In situ ATR FTIR studies of SO4 adsorption on goethite in the presence of copper ions. Environ. Sci. Technol. 42, 9191–9196.
Benjamin, M.M., Leckie, J.O., 1982. Effects of complexation by cl, SO4, and S2O3 on adsorption behavior of cd on oxide-surfaces. Environ. Sci. Technol. 16, 162–170.
Bian, Z.F., Miao, X.X., Lei, S.G., Chen, S.E., Wang, W.F., Struthers, S., 2012. The challenges of reusing mining and mineral-processing wastes. Science 337, 702–703.
Boily, J., Fein, J.B., 1996. Experimental study of cadmium-citrate co-adsorption onto α-Al2O3. Geochim. Cosmochim. Acta 60 (16), 2929–2938.
Boily, J.F., Sjöberg, S., Persson, P., 2005. Structures and stabilities of Cd(II) and Cd(II)-phthalate complexes at the goethite/water interface. Geochim. Cosmochim. Acta 69 (13), 3219–3235.
Bolland, M.D.A., Posner, A.M., Quirk, J.P., 1977. Zinc adsorption by goethite in the absence and presence of phosphate. Aust. J. Soil Res. 15, 279–286.
Boyle-Wight, E.J., Katz, L.E., Hayes, K.F., 2002a. Macroscopic studies of the effects of selenate and selenite on cobalt sorption to γ-Al2O3. Environ. Sci. Technol. 36 (6), 1212–1218.
Boyle-Wight, E.J., Katz, L.E., Hayes, K.F., 2002b. Spectroscopic studies of the effects of selenate and selenite on cobalt sorption to γ-Al2O3. Environ. Sci. Technol. 36 (6), 1219–1225.
Buerge-Weirich, D., Behra, P., Sigg, L., 2003. Adsorption of copper, nickel, and cadmium on goethite in the presence of organic ligands. Aquat. Geochem. 9, 65–85.
Cao, X., Ma, L.Q., Chen, M., Singh, S.P., Harris, W.G., 2002. Impacts of phosphate amendments on lead biogeochemistry at a contaminated site. Environ. Sci. Technol. 36, 5296–5304.
Carabante, I., Grahn, M., Holmgren, A., Kumpiene, J., Hedlund, J., 2012. Influence of Zn(II) on the adsorption of arsenate onto ferrihydrite. Environ. Sci. Technol. 46 (24), 13152–13159.
Catalano, J.G., Luo, Y., Otemuyiwa, B., 2011. Effect of aqueous Fe(II) on arsenate sorption on goethite and hematite. Environ. Sci. Technol. 45, 8826–8833.
Cheng, T., Barnett, M.O., Roden, E.E., Zhuang, J., 2004. Effects of phosphate on Uranium(VI) adsorption to goethite-coated sand. Environ. Sci. Technol. 38 (22), 6059–6065.
Chrysochoou, M., Dermatas, D., Grubb, D.G., 2007. Phosphate application to firing range soils for pb immobilization: the unclear role of phosphate. J. Hazard. Mater. 144 (1–2), 1–14.
Collins, C.R., Ragnarsdottir, K.V., Sherman, D.M., 1999. Effect of inorganic and organic ligands on the mechanism of cadmium sorption to goethite. Geochim. Cosmochim. Acta 63, 2989–3002.
Comarmond, M.J., Steudtner, R., Stockmann, M., Heim, K., Müller, K., Brendler, V., Payne, T.E., Foerstendorf, H., 2016. The sorption processes of U(VI) onto SiO2 in the presence of phosphate: from binary surface species to precipitation. Environ. Sci. Technol. 50 (21), 11610–11618.
Cui, Y., Du, X., Weng, L., Van Riemsdijk, W.H., 2010. Assessment of in situ immobilization of Lead (Pb) and arsenic (As) in contaminated soils with phosphate and iron: solubility and bioaccessibility. Water Air Soil Pollut. 213 (1–4), 95–104.
Del Nero, M., Galindo, C., Barillon, R., Madé, B., 2011. TRLFS evidence for precipitation of uranyl phosphate on the surface of alumina: environmental implications. Environ. Sci. Technol. 45, 3982–3988.
Diaz-Barrientos, E., Madrid, L., Contreras, M.C., Morillo, E., 1990. Simultaneous adsorption of zinc and phosphate on synthetic lepidocrocite. Aust. J. Soil Res. 28 (4), 549–557.
Elzinga, E.J., Kretzschmar, R., 2013. In situ ATR-FTIR spectroscopic analysis of the co-adsorption of orthophosphate and Cd(II) onto hematite. Geochim. Cosmochim. Acta 117 (1), 53–64.
Elzinga, E.J., Peak, D., Sparks, D.L., 2001. Spectroscopic studies of Pb(II)-sulfate interactions at the goethite-water interface. Geochim. Cosmochim. Acta 65 (14), 2219–2230.
Elzinga, E.J., Tang, Y.Z., McDonald, J., DeSisto, S., Reeder, R.J., 2009. Macroscopic and spectroscopic characterization of selenate, selenite, and chromate adsorption at the solid-water interface of γ-Al2O3. J. Colloid Interface Sci. 340 (2), 153–159.
Estrada, C.F., Sverjensky, D.A., Hazen, R.M., 2019. Selective adsorption of aspartate facilitated by calcium on brucite [Mg(OH)2]. ACS Earth Space Chem. 3, 1–7.
Fitts, J.P., Persson, P., Brown Jr., G.E., Parks, G.A., 1999. Structure and bonding of Cu(II)–glutamate complexes at the γ-Al2O3–water interface. J. Colloid Interface Sci. 220 (1), 133–147.
Floroiu, R.M., Davis, A.P., Torrents, A., 2001. Cadmium adsorption on aluminum oxide in the presence of polyacrylic acid. Environ. Sci. Technol. 35 (2), 348–353.
Flynn, E.D., Catalano, J.G., 2017. Competitive and cooperative effects during nickel adsorption to iron oxides in the presence of oxalate. Environ. Sci. Technol. 51 (17), 9792–9799.
Foster, A.L., Brown, G.E., Parks, G.A., 2003. X-ray absorption fine structure study of As (V) and Se(IV) sorption complexes on hydrous mn oxides. Geochim. Cosmochim. Acta 67 (11), 1937–1953.
Galindo, C., Nero, M.D., Barillon, R., Halter, E., Made, B., 2010. Mechanisms of uranyl and phosphate (co)sorption: complexation and precipitation at α-Al2O3 surfaces. J. Colloid Interface Sci. 347, 282–289.
Gao, Y.Z., He, J.Z., Ling, W.T., Hu, H.Q., Liu, F., 2003. Effects of organic acids on copper and cadmium desorption from contaminated soils. Environ. Int. 29, 613–618.
Ghanem, S.A., Mikkelson, D.S., 1988. Sorption of zinc on iron hydrous oxide. Soil Sci. 146, 11–21.
Gräfe, M., Beattie, D.A., Smith, E., Skinner, W.M., Singh, B., 2008a. Copper and arsenate co-sorption at the mineral–water interfaces of goethite and jarosite. J. Colloid Interface Sci. 322, 399–413.
Gräfe, M., Nachtegaal, M., Sparks, D.L., 2004. Formation of metal-arsenate precipitates at the goethite-water interface. Environ. Sci. Technol. 38 (24), 6561–6570.
Gräfe, M., Sparks, D.L., 2005. Kinetics of zinc and arsenate co-sorption at the goethite–water interface. Geochim. Cosmochim. Acta 69, 4573–4595.
Gräfe, M., Tappero, R.V., Marcus, M.A., Sparks, D.L., 2008b. Arsenic speciation in multiple metal environments: I. bulk-XAFS spectroscopy of model and mixed compounds. J. Colloid Interface Sci. 320, 383–399.
Ha, J., Trainor, T.P., Farges, F., Brown, G.E., 2009. Interaction of Zn(II) with hematite nanoparticles and microparticles: part 2. ATR-FTIR and EXAFS study of the aqueous Zn(II)/oxalate/hematite ternary system. Langmuir 25 (10), 5586–5593.
Hayes, K.F., Roe, A.L., Brown, G.E., Hodgson, K.O., Leckie, J.O., Parks, G.A., 1987. In situ X-ray absorption study of surface complexes: selenium oxyanions on a-FeOOH. Science 238 (4828), 783–786.
Hafsteinsdóttir, E.G., Camenzuli, D., Rocavert, A.L., Walworth, J., Gore, D.B., 2015. Chemical immobilization of metals and metalloids by phosphates. Appl. Geochem. 59, 47–62.
Hamidpour, M., Karamooz, M., Akhgar, A., Tajabadipour, A., Furrer, G., 2019. Adsorption of cd and zn onto micaceous minerals-effect of siderophore desferrioxamine B. Pedosphere 29 (5), 590–597.
Hawke, D., Carpenter, P.D., Hunter, K.A., 1989. Competitive adsorption of phosphate on goethite in marine electrolytes. Environ. Sci. Technol. 23, 187–191.
Hébert, M., Fugère, V., Gonzalez, A., 2019. The overlooked impact of rising glyphosate use on phosphorus loading in agricultural watersheds. Front. Ecol. Environ. 17 (1), 48–56.
Hinkle, M.A.G., Wang, Z., Giammar, D.E., Catalano, J.G., 2015. Interaction of Fe(II) with phosphate and sulfate on iron oxide surfaces. Geochim. Cosmochim. Acta 158, 130–146.
Hoins, U., 1993. Ligand effect on the adsorption of heavy metals: the sulfate-cadmium-goethite case. Water Air Soil Pollut. 68 (1–2), 241–255.
Hu, S., Lian, F., Wang, J., 2019. Effect of pH to the surface precipitation mechanisms of arsenate and cadmium on TiO2. Sci. Total Environ. 666, 956–963.
Hu, S., Yan, L., Chan, T., Jing, C., 2015. Molecular insights into ternary surface complexation of arsenite and cadmium on TiO2. Environ. Sci. Technol. 49, 5973–5979.
Huang, G., Su, X., Rizwan, M.S., Zhu, Y., Hu, H., 2016. Chemical immobilization of pb, cu, and cd by phosphate materials and calcium carbonate in contaminated soils. Environ. Sci. Pollut. Res. 23 (16), 16845–16856.
Huang, L., Hu, H., Li, X., Li, L.Y., 2010. Influences of low molar mass organic acids on the adsorption of Cd2+ and Pb2+ by goethite and montmorillonite. Appl. Clay Sci. 49 (3), 281–287.
Jiang, W., Lv, J., Luo, L., Yang, K., Lin, Y., Hu, F., Zhang, J., Zhang, S., 2013. Arsenate and cadmium co-adsorption and co-precipitation on goethite. J. Hazard. Mater. 262, 55–63.
Jordan, N., Ritter, A., Scheinost, A.C., Weiss, S., Schild, D., Hubner, R., 2014. Selenium(IV) uptake by maghemite (γ-Fe_2O_3). Environ. Sci. Technol. 48, 1665–1674.
Juang, R., Chung, J., 2004. Equilibrium sorption of heavy metals and phosphate from single- and binary-sorbate solutions on goethite. J. Colloid Interface Sci. 275 (1), 53–60.
Juang, R., Wu, W., 2002. Adsorption of sulfate and copper(II) on goethite in relation to the changes of zeta potentials. J. Colloid Interface Sci. 249 (1), 22–29.
Kappler, A., Bryce, C., Mansor, M., Lueder, U., Byrne, J.M., Swanner, E.D., 2021. An evolving view on biogeochemical cycling of iron. Nat. Rev. Microbiol. 19, 360–374.
Karimzadeh, L., Lippmann-Pipke, J., Franke, K., Lippold, H., 2017. Mobility and transport of copper(II) influenced by the microbial siderophore DFOB: column experiment and modelling. Chemosphere 173, 326–329.
Karimzadeh, L., Nair, S., Merkel, B.J., 2013. Effect of microbial siderophore DFOB on pb, zn, and cd sorption onto zeolite. Aquat. Geochem. 19 (1), 25–37.
Kim, C.S., Rytuba, J.J., Brown, G.E., 2004. EXAFS study of mercury(II) sorption to fe- and Al-(hydr)oxides: II. effects of chloride and sulfate. J. Colloid Interface Sci. 270 (1), 9–20.
Kim, J.-Y., Davis, A.P., Kim, K.-W., 2003. Stabilization of available arsenic in highly contaminated mine tailings using iron. Environ. Sci. Technol. 37 (1), 189–195.
Kraemer, S.M., Xu, J., Raymond, K.N., Sposito, G., 2002. Adsorption of Pb(II) and Eu(III) by oxide minerals in the presence of natural and synthetic hydroxamate siderophores. Environ. Sci. Technol. 36 (6), 1287–1291.
Kumar, E., Bhatnagar, A., Hogland, W., Marques, M., Sillanpää, M., 2014a. Interaction of anionic pollutants with Al-based adsorbents in aqueous media – a review. Chem. Eng. J. 241, 443–456.

Kumar, E., Bhatnagar, A., Hogland, W., Marques, M., Sillanpää, M., 2014b. Interaction of inorganic anions with iron-mineral adsorbents in aqueous media – a review. Adv. Colloid Interf. Sci. 203, 11–21.
Kushwaha, A., Goswami, L., Lee, J., Sonne, C., Brown, R.J.C., Kim, K., 2021. Selenium in soil-microbe-plant systems: sources, distribution, toxicity, tolerance, and detoxification. Crit. Rev. Environ. Sci. Technol.. https://doi.org/10.1080/10643389.2021.1883187.
Lackovic, K., Angove, M.J., Wells, J.D., Johnson, B.B., 2004. Modeling the sorption of cd onto goethite in the presence of citric acid. J. Colloid Interface Sci. 269, 37–45.
Lamers, L.P.M., Tomassen, H.B.M., Roelofs, J.G.M., 1998. Sulfate-induced eutrophication and phytotoxicity in freshwater wetlands. Environ. Sci. Technol. 32 (2), 199–205.
Lee, N., Sverjensky, D.A., Hazen, R.M., 2014. Cooperative and competitive adsorption of amino acids with Ca2+ on rutile (α-TiO2). Environ. Sci. Technol. 48, 9358–9365.
Lenhart, J.J., Bargar, J.R., Davis, J.A., 2001. Spectroscopic evidence for ternary surface complexes in the lead(II)-malonic acid-hematite system. J. Colloid Interface Sci. 234, 448–452.
Li, S.W., Liu, X., Sun, H.J., Li, M.Y., Zhao, D., Luo, J., Li, H.B., Ma, L.Q., 2017. Effect of phosphate amendment on relative bioavailability and bioaccessibility of lead and arsenic in contaminated soils. J. Hazard. Mater. 339, 256–263.
Li, W., Feng, X., Yan, Y., Sparks, D.L., Phillips, B.L., 2013a. Solid-state NMR spectroscopic study of phosphate sorption mechanisms on aluminum (hydr)oxides. Environ. Sci. Technol. 47, 8308–8315.
Li, W., Harrington, R., Tang, Y., Kubicki, J.D., Aryanpour, M., Reeder, R.J., Parise, J.B., Phillips, B.L., 2011. Differential pair distribution function study of the structure of arsenate adsorbed on nanocrystalline γ-alumina. Environ. Sci. Technol. 45, 9687–9692.
Li, W., Wang, Y.J., Zhu, M.Q., Fan, T.T., Zhou, D.M., Phillips, B.L., Sparks, D.L., 2013b. Inhibition mechanisms of zn precipitation on aluminum oxide by glyphosate: a 31P NMR and zn EXAFS study. Environ. Sci. Technol. 47, 4211–4219.
Li, W., Xu, W.Q., Parise, J.B., Phillips, B.L., 2012. Formation of hydroxylapatite from co-sorption of phosphate and calcium by boehmite. Geochim. Cosmochim. Acta 85, 289–301.
Li, W., Zhang, S., Jiang, W., Shan, X., 2006. Effect of phosphate on the adsorption of Cu and Cd on natural hematite. Chemosphere 63, 1235–1241.
Li, W., Zhang, S., Shan, X.Q., 2007. Surface modification of goethite by phosphate for enhancement of Cu and Cd adsorption. Colloids Surf. A Physicochem. Eng. Asp. 293, 13–19.
Liang, J., Xu, R., Jiang, X., Wang, Y., Zhao, A., Tan, W., 2007a. Effect of arsenate on adsorption of Cd(II) by two variable charge soils. Chemosphere 67 (10), 1949–1955.
Liang, J., Xu, R., Tiwari, D., Zhao, A., 2007b. Effect of arsenate on adsorption of Zn(II) by three variable charge soils. Soil Res. 45 (6), 465–472.
Lin, J., Zhan, Y., Wang, H., Chu, M., Wang, C., He, Y., Wang, X., 2017. Effect of calcium ion on phosphate adsorption onto hydrous zirconium oxide. Chem. Eng. J. 309, 118–129.
Lin, S.H., Kao, H.C., Cheng, C.H., Juang, R.S., 2004. An EXFAS study of the structures of copper and phosphate sorbed onto goethite. Colloids Surf. A Physicochem. Eng. Asp. 234, 71–75.
Liu, R.Q., Zhao, D.Y., 2007. In situ immobilization of Cu(II) in soils using a new class of iron phosphate nanoparticles. Chemosphere 68 (10), 1867–1876.
Liu, J., Zhu, R., Liang, X., Ma, L., Lin, X., Zhu, J., He, H., Parker, S.C., Molinari, M., 2018. Synergistic adsorption of Cd(II) with sulfate/phosphate on ferrihydrite: an in situ ATR-FTIR/2D-COS study. Chem. Geol. 477, 12–21.
Liu, J., Zhu, R., Ma, L., Fu, H., Lin, X., Parker, S.C., Molinari, M., 2021. Adsorption of phosphate and cadmium on iron (oxyhydr)oxides: a comparative study on ferrihydrite, goethite, and hematite. Geoderma 383, 114799.
Liu, J., Zhu, R., Xu, T., Xu, Y., Ge, F., Xi, Y., Zhu, J., He, H., 2016. Co-adsorption of phosphate and zinc(II) on the surface of ferrihydrite. Chemosphere 144, 1148–1155.
Loring, J.S., Sandström, M.H., Noén, K., Persson, P., 2009. Rethinking arsenate coordination at the surface of goethite. Chem. Eur. J. 15, 5063–5072.
Madrid, L., Diaz-Barrientos, E., Contreras, M.C., 1991. Relationships between zinc and phosphate adsorption on montmorillonite and an iron oxyhydroxide. Aust. J. Soil Res. 29 (2), 239–247.
Marcussen, H., Holm, P.E., Strobel, B.W., Hansen, H.C.B., 2009. Nickel sorption to goethite and montmorillonite in presence of citrate. Environ. Sci. Technol. 43 (4), 1122–1127.
Masue, Y., Loeppert, R.H., Kramer, T.A., 2007. Arsenate and arsenite adsorption and desorption behavior on coprecipitated aluminum: iron hydroxides. Environ. Sci. Technol. 41, 837–842.
Mauric, A., Lottermoser, B.G., 2011. Phosphate amendment of metalliferous waste rocks, century Pb–Zn mine, Australia: laboratory and field trials. Appl. Geochem. 26, 45–56.
McBride, M.B., 1985. Influence of glycine on Cu2+ adsorption by microcrystalline gibbsite and boehmite. Clay Clay Miner. 33 (5), 397–402.
Mei, H., Tan, X., Yu, S., Ren, X., Chen, C., Wang, X., 2015. Effect of silicate on U(VI) sorption to γ-Al2O3: batch and EXAFS studies. Chem. Eng. J. 269, 371–378.
Miretzky, P., Fernandez-Cirelli, A., 2008. Phosphates for pb immobilization in soils: a review. Environ. Chem. Lett. 6, 121–133.
Mehta, V.S., Maillot, F., Wang, Z., Catalano, J.G., Giammar, D.E., 2016. Effect of reaction pathway on the extent and mechanism of Uranium(VI) immobilization with calcium and phosphate. Environ. Sci. Technol. 50 (6), 3128–3136.
Mendez, J.C., Hiemstra, T., 2020. Ternary complex formation of phosphate with ca and mg ions binding to ferrihydrite: experiments and mechanisms. ACS Earth Space Chem. 4 (4), 545–557.
Mishra, B., Haack, E.A., Maurice, P.A., Bunker, B.A., 2010. A spectroscopic study of the effects of a microbial siderophore on pb adsorption to kaolinite. Chem. Geol. 275 (3–4), 199–207.
Mohan, D., Pittman, C.U., 2007. Arsenic removal from water/wastewater using adsorbents—a critical review. J. Hazard. Mater. 142, 1–53.
Morillo, E., Undabeytia, T., Maqueda, C., 1997. Adsorption of glyphosate on the clay mineral montmorillonite: effect of Cu(II) in solution and adsorbed on the mineral. Environ. Sci. Technol. 31 (12), 3588–3592.
Mustafa, S., Zaman, M.I., Rana, G., Khan, S., 2008. Effect of Ni2+ loading on the mechanism of phosphate anion sorption by iron hydroxide. Separ. Purif. Technol. 59, 108–114.
Nakajima, K., Takeda, O., Miki, T., Matsubae, K., Nagasaka, T., 2011. Thermodynamic analysis for the controllability of elements in the recycling process of metals. Environ. Sci. Technol. 45, 4929–4936.
Nelson, H., Sjöberg, S., Lövgren, L., 2013. Surface complexation modelling of arsenate and copper adsorbed at the goethite/water interface. Appl. Geochem. 35, 64–74.
Net, S., Delmont, A., Sempéré, R., Paluselli, A., Ouddane, B., 2015. Reliable quantification of phthalates in environmental matrices (air, water, sediment, sludge and soil): a review. Sci. Total Environ. 515–516, 162–180.
Nie, Z., Finck, N., Heberling, F., Pruessmann, T., Liu, C., Lützenkirchen, J., 2017. Adsorption of selenium and strontium on goethite: EXAFS study and surface complexation modeling of the ternary systems. Environ. Sci. Technol. 51 (7), 3751–3758.
Neubauer, U., Furrer, G., Schulin, R., 2002. Heavy metal sorption on soil minerals affected by the siderophore desferrioxamine B: the role of Fe(III) (hydr)oxides and dissolved Fe(III). Eur. J. Soil Sci. 53, 45–55.
Neubauer, U., Nowack, B., Furrer, G., Schulin, R., 2000. Heavy metal sorption on clay minerals affected by the siderophore desferrioxamine B. Environ. Sci. Technol. 34, 2749–2755.
Obrycki, J.F., Scheckel, K.G., Basta, N.T., 2017. Soil solution interactions may limit pb remediation using P amendments in an urban soil. Environ. Pollut. 220, 549–556.
Ostergren, J.D., Brown, G.E., Parks, G.A., Persson, P., 2000a. Inorganic ligand effects on Pb (II) sorption to goethite (α-FeOOH): II. Sulfate. J. Colloid Interface Sci. 225, 483–493.
Ostergren, J.D., Trainor, T.P., Bargar, J.R., Brown, G.E., Parks, G.A., 2000b. Inorganic ligand effects on Pb(II) sorption to goethite (α-FeOOH): I. Carbonate. J. Colloid Interface Sci. 225 (2), 466–482.
Peak, D., Sparks, D.L., 2002. Mechanisms of selenate adsorption on iron oxides and hydroxides. Environ. Sci. Technol. 36 (7), 1460–1466.
Peiffer, S., Kappler, A., Haderlein, S.B., Schmidt, C., Byrne, J.M., Kleindienst, S., Vogt, C., Richnow, H.H., Obst, M., Angenent, L.T., Bryce, C., McCammon, C., Planer-Friedrich, B., 2021. A Biogeochemical–hydrological framework for the role of redox-active compounds in aquatic systems. Nat. Geosci. 14 (5), 264–272.
Pérez-Novo, C., Bermúdez-Couso, A., López-Periago, E., Fernández-Calviño, D., Arias-Estévez, M., 2009. The effect of phosphate on the sorption of copper by acid soils. Geoderma 150, 166–170.
Pérez-Novo, C., Bermúdez-Couso, A., López-Periago, E., Fernández-Calviño, D., Arias-Estévez, M., 2011. Zinc adsorption in acid soils influence of phosphate. Geoderma 162, 358–364.
Putnis, C.V., Ruiz-Agudo, E., 2013. The mineral-water Interface: where minerals react with the environment. Elements 9, 177–182.
Ramstedt, M., Norgren, C., Shchukarev, A., Sjöberg, S., Persson, P., 2005. Co-adsorption of cadmium(II) and glyphosate at the water–manganite (?-MnOOH) interface. J. Colloid Interface Sci. 285 (2), 493–501.
Raven, K.P., Jain, A., Loeppert, R.H., 1998. Arsenite and arsenate adsorption on ferrihydrite: kinetics, equilibrium, and adsorption envelopes. Environ. Sci. Technol. 32, 344–349.
Ren, H., Jia, S., Liu, Y., Wu, S., Han, X., 2012a. Effects of Mn(II) on the sorption and mobilization of As(V) in the presence of hematite. J. Hazard. Mater. 217–218, 301–306.
Ren, X., Yang, S., Tan, X., Chen, C., Sheng, G., Wang, X., 2012b. Mutual effects of copper and phosphate on their interaction with γ-Al_2O_3: combined batch macroscopic experiments with DFT calculations. J. Hazard. Mater. 237–238, 199–208.
Ren, X., Tan, X., Hayat, T., Alsaedi, A., Wang, X., 2015. Co-sequestration of Zn(II) and phosphate by γ-Al2O3: from macroscopic to microscopic investigation. J. Hazard. Mater. 297, 134–145.
Rietra, R.P.J.J., Hiemstra, T., van Riemsdijk, W.H., 2001. Interaction between calcium and phosphate adsorption on goethite. Environ. Sci. Technol. 35, 3369–3374.
Ruyter-Hooley, M., Johnson, B.B., Morton, D.W., Angove, M.J., 2017. The adsorption of myo-inositol hexaphosphate onto kaolinite and its effect on cadmium retention. Appl. Clay Sci. 135, 405–413.
Ruyter-Hooley, M., Larsson, A.-C., Johnson, B.B., Antzutkin, O.N., Angove, M.J., 2016. The effect of inositol hexaphosphate on cadmium sorption to gibbsite. J. Colloid Interface Sci. 474, 159–170.
Saha, M., Sarkar, S., Sarkar, B., Sharma, B.K., Bhattacharjee, S., Tribedi, P., 2016. Microbial siderophores and their potential applications: a review. Environ. Sci. Pollut. Res. 23 (5), 3984–3999.
Scheckel, K.G., Ryan, J.A., 2004. Spectroscopic speciation and quantification of lead in phosphate-amended soils. J. Environ. Qual. 33 (4), 1288–1295.
Shahid, M., Pinelli, E., Dumat, C., 2012. Review of pb availability and toxicity to plants in relation with metal speciation; role of synthetic and natural organic ligands. J. Hazard. Mater. 219–220, 1–12.
Sheals, J., Granström, M., Sjöberg, S., Persson, P., 2003. Coadsorption of Cu(II) and glyphosate at the water–goethite (a-FeOOH) interface: molecular structures from FTIR and EXAFS measurements. J. Colloid Interface Sci. 262 (1), 38–47.
Shirvani, M., Shariatmadari, H., Kalbasi, M., Nourbakhsh, F., Najafi, B., 2006. Sorption of cadmium on palygorskite, sepiolite and calcite: equilibria and organic ligand affected kinetics. Colloids Surf. A Physicochem. Eng. Asp. 287 (1–3), 182–190.
Simanova, A.A., Loring, J.S., Persson, P., 2011. Formation of ternary metal-oxalate surface complexes on a-FeOOH particles. J. Phys. Chem. C 115, 21191–21198.
Singh, A., Catalano, J.G., Ulrich, K., Giammar, D.E., 2012. Molecular-scale structure of Uranium(VI) immobilized with goethite and phosphate. Environ. Sci. Technol. 46, 6594–6603.
Singh, A., Ulrich, K., Giammar, D.E., 2010. Impact of phosphate on U(VI) immobilization in the presence of goethite. Geochim. Cosmochim. Acta 74, 6324–6343.
Singh, R., Singh, S., Parihar, P., Singh, V.P., Prasad, S.M., 2015. Arsenic contamination, consequences and remediation techniques: a review. Ecotoxicol. Environ. Saf. 112, 247–270.

Smith, E., Naidu, R., Alston, A.M., 1998. Arsenic in the soil environment: a review. Adv. Agron. 64, 149–195.
Song, Y., Swedlund, P.J., Singhal, N., 2008. Copper(II) and cadmium(II) sorption onto ferrihydrite in the presence of phthalic acid: some properties of the ternary complex. Environ. Sci. Technol. 42 (11), 4008–4013.
Song, Y., Swedlund, P.J., Singhal, N., Swift, S., 2009. Cadmium(II) speciation in complex aquatic systems: a study with ferrihydrite, bacteria, and an organic ligand. Environ. Sci. Technol. 43, 7430–7436.
Sparks, D.L., 2014. Advances in coupling of kinetics and molecular scale tools to shed light on soil biogeochemical processes. Plant Soil 387, 1–19.
Sparks, D.L., 2002. Environmental Soil Chemistry. Second edition. Academic Press, Boston.
Sparks, D.L., 2005. Toxic metals in the environment: the role of surfaces. Elements 1, 193–197.
Stietiya, M.H., Wang, J.J., 2014. Zinc and cadmium adsorption to aluminum oxide nanoparticles affected by naturally occurring ligands. J. Environ. Qual. 43 (2), 498–506.
Stietiya, M.H., Wang, J.J., Roy, A., 2011. Macroscopic and extended X-ray absorption fine structure spectroscopic investigation of ligand effect on zinc adsorption to kaolinite as a function of pH. Soil Sci. 176 (9), 464–471.
Swedlund, P.J., Webster, J.G., 2001. Cu and zn ternary surface complex formation with SO4 on ferrihydrite and schwertmannite. Appl. Geochem. 16, 503–511.
Swedlund, P.J., Webster, J.G., Miskelly, G.M., 2003. The effect of SO4 on the ferrihydrite adsorption of Co, Pb and Cd: ternary complexes and site heterogeneity. Appl. Geochem. 18, 1671–1689.
Swedlund, P.J., Webster, J.G., Miskelly, G.M., 2009. Goethite adsorption of Cu(II), Pb(II), Cd (II), and Zn(II) in the presence of sulfate: properties of the ternary complex. Geochim. Cosmochim. Acta 73, 1548–1562.
Tan, X., Fang, M., Ren, X., Mei, H., Shao, D., Wang, X., 2014. Effect of silicate on the formation and stability of ni-Al LDH at γ-Al2O3 surface. Environ. Sci. Technol. 48, 13138–13145.
Tang, Y., Werth, C.J., Sanford, R.A., Singh, R., Michelson, K., Nobu, M., Liu, W.-T., Valocchi, A.J., 2015. Immobilization of selenite via two parallel pathways during in situ bioremediation. Environ. Sci. Technol. 49 (7), 4543–4550.
Taylor, R.W., Bleam, W.F., Ranatunga, T.D., Schulthess, C.P., Senwo, Z.N., Ranatunga, D.R.A., 2009. X-ray absorption near edge structure study of lead sorption on phosphate-treated kaolinite. Environ. Sci. Technol. 43, 711–717.
Theis, T.L., West, M.J., 1986. Effects of cyanide complexation on adsorption of trace metals at the surface of goethite. Environ. Technol. Lett. 7, 309–318.
ThomasArrigo, L.K., Byrne, J.M., Kappler, A., Ruben Kretzschmar, R., 2018. Impact of organic matter on iron(II)-catalyzed mineral transformations in ferrihydrite–organic matter coprecipitates. Environ. Sci. Technol. 52 (21), 12316–12326.
ThomasArrigo, L.K., Mikutta, C., Byrne, J., Kappler, A., Kretzschmar, R., 2017. Iron(II)-catalyzed iron atom exchange and mineralogical changes in iron-rich organic freshwater flocs: an iron isotope tracer study. Environ. Sci. Technol. 51 (12), 6897–6907.
Tiberg, C., Gustafsson, J.P., 2016. Phosphate effects on cadmium(II) sorption to ferrihydrite. J. Colloid Interface Sci. 471, 103–111.
Tiberg, C., Sjöstedt, C., Persson, I., Gustafsson, J.P., 2013. Phosphate effects on copper(II) and lead(II) sorption to ferrihydrite. Geochim. Cosmochim. Acta 120, 140–157.
Troyer, L.D., Maillot, F., Wang, Z., Wang, Z., Mehta, V.S., Giammar, D.E., Catalano, J.G., 2016. Effect of phosphate on U(VI) sorption to montmorillonite: ternary complexation and precipitation barriers. Geochim. Cosmochim. Acta 175, 86–99.
Turner, B.L., Papházy, M.J., Haygarth, P.M., McKelvie, I.D., 2002. Inositol phosphates in the environment. Phil. Trans. R. Soc. Lond. B 357, 449–469.
Venema, P., Hiemstra, T., van Riemsdijk, W.H., 1997. Interaction of cadmium with phosphate on goethite. J. Colloid Interface Sci. 192, 94–103.
Villalobos, M., Trotz, M.A., Leckie, J.O., 2001. Surface complexation modeling of carbonate effects on the adsorption of Cr(VI), Pb(II), and U(VI) on goethite. Environ. Sci. Technol. 35 (19), 3849–3856.
Violante, A., Ricciardella, M., Pigna, M., 2003. Adsorption of heavy metals on mixed Fe–Al oxides in the absence or presence of organic ligands. Water Air Soil Pollut. 145, 289–306.
Wan, B., Yan, Y.P., Zhu, M.Q., Wang, X.M., Liu, F., Tan, W.F., Feng, X.H., 2017. Quantitative and spectroscopic investigations of the co-sorption of myo-inositol hexakisphosphate and cadmium(II) onto haematite. Eur. J. Soil Sci. 68, 374–383.
Wang, C., Cui, Y., Zhang, J.H., Gomez, M., Wang, S.F., Jia, Y.F., 2018. Occurrence state of coexisting arsenate and nickel ions at the ferrihydrite-water interface: mechanisms of surface complexation and surface precipitation via ATR-IR spectroscopy. Chemosphere 206, 33–42.
Wang, K., Xing, B., 2002. Adsorption and desorption of cadmium by goethite pretreated with phosphate. Chemosphere 48, 665–670.
Wang, K., Xing, B., 2004. Mutual effects of cadmium and phosphate on their adsorption and desorption by goethite. Environ. Pollut. 127, 13–20.
Wang, L., Putnis, C.V., Ruiz-Agudo, E., King, H.E., Putnis, A., 2013. Coupled dissolution and precipitation at the cerussite-phosphate solution Interface: implications for immobilization of Lead in soils. Environ. Sci. Technol. 47 (23), 13502–13510.
Wang, X., Li, W., Harrington, R., Liu, F., Parise, J.B., Feng, X., Sparks, D.L., 2013. Effect of ferrihydrite crystallite size on phosphate adsorption reactivity. Environ. Sci. Technol. 47, 10322–10331.
Wang, X., Zhang, H., Wang, L., Chen, J., Xu, S., Hou, H., Shi, Y., Zhang, J., Ma, M., Tsang, D.C.W., Crittenden, J.C., 2019. Transformation of arsenic during realgar tailings stabilization using ferrous sulfate in a pilot-scale treatment. Sci. Tot. Environ. 668, 32–39.
Wang, Y.J., Fan, T.T., Liu, C., Li, W., Zhu, M.Q., Fan, J.X., Gong, H., Zhou, D.M., Sparks, D.L., 2017. Macroscopic and microscopic investigation of adsorption and precipitation of zn on gamma-alumina in the absence and presence of as. Chemosphere 178, 309–316.
Wang, Y.J., Zhou, D.M., Sun, R.J., Jia, D.A., Zhu, H.W., Wang, S.Q., 2008. Zinc adsorption on goethite as affected by glyphosate. J. Hazard. Mater. 151 (1), 179–184.
Weesner, F.J., Bleam, W.F., 1998. Binding characteristics of Pb2+ on anion-modified and pristine hydrous oxide surfaces studied by electrophoretic mobility and X-ray absorption spectroscopy. J. Colloid Interface Sci. 205, 380–389.
Xenidis, A., Stouraiti, C., Papassiopi, N., 2010. Stabilization of pb and as in soils by applying combined treatment with phosphates and ferrous iron. J. Hazard. Mater. 177 (1–3), 929–937.
Xie, L., Giammar, D.E., 2007. Influence of phosphate on adsorption and surface precipitation of lead on iron oxide surfaces. In: Barnett, M.O., Kent, D.O. (Eds.), Adsorption of Metals by Geomedia II: Variables, Mechanisms, and Model Applications. Elsevier, Amsterdam, Netherlands.
Yamaguchi, N.U., Scheinost, A.C., Sparks, D.L., 2002. Influence of gibbsite surface area and citrate on ni sorption mechanisms at pH 7.5. clay. Clay Miner. 50 (6), 784–790.
Yamaguchi, N.U., Scheinost, A.C., Sparks, D.L., 2001. Surface-induced nickel hydroxide precipitation in the presence of citrate and salicylate. Soil Sci. Soc. Am. J. 65, 729–736.
Yan, Y., Li, W., Yang, J., Zheng, A., Liu, F., Feng, X., Sparks, D.L., 2014. Mechanism of myo-inositol hexakisphosphate sorption on amorphous aluminum hydroxide: spectroscopic evidence for rapid surface precipitation. Environ. Sci. Technol. 48 (12), 6735–6742.
Yan, Y., Wan, B., Jaisi, D.P., Yin, H., Hu, Z., Wang, X., Chen, C., Liu, F., Tan, W., Feng, X., 2018a. Effects of myo-inositol hexakisphosphate on Zn(II) sorption on γ-alumina: a mechanistic study. ACS Earth Space Chem. 2 (8), 787–796.
Yan, Y., Wan, B., Zhang, Y., Zhang, L., Liu, F., Feng, X., 2018b. In situ ATR-FTIR spectroscopic study of the co-adsorption of myo-inositol hexakisphosphate and Zn(II) onto goethite. Soil Res. 56, 526–534.
Yang, W., Kan, A.T., Chen, W., Tomson, M.B., 2010. PH-dependent effect of zinc on arsenic adsorption to magnetite nanoparticles. Water Res. 44, 5693–5701.
Yang, X., Liu, L., Tan, W., Liu, C., Dang, Z., Qiu, G., 2020. Remediation of heavy metal contaminated soils by organic acid extraction and electrochemical adsorption. Environ. Pollut. 264, 114745.
Yang, Y., Wang, S., Liu, J., Xu, Y., Zhou, X., 2016. Adsorption of lysine on na-montmorillonite and competition with Ca2+: a combined XRD and ATR-FTIR study. Langmuir 32, 4746–4754.
Yao, W., Millero, F.J., 1996. Adsorption of phosphate on manganese dioxide in seawater. Environ. Sci. Technol. 30, 536–541.
Yoon, S.J., Helmke, P.A., Amonette, J.E., Bleam, W.F., 2002. X-ray absorption and magnetic studies of trivalent lanthanide sorbed on pristine and phosphate-modified boehmite surfaces. Langmuir 18, 10128–10136.
Yoshida, T., Ozaki, T., Ohnuki, T., Francis, A.J., 2004. Adsorption of rare earth elements by γ-Al2O3 and Pseudomonas fluorescens cells in the presence of desferrioxamine B: implication of siderophores for the ce anomaly. Chem. Geol. 212 (3–4), 239–246.
Yu, H., Wang, X., Li, F., Li, B., Liu, C., Wang, Q., Lei, J., 2017. Arsenic mobility and bioavailability in paddy soil under iron compound amendments at different growth stages of rice. Environ. Pollut. 224, 136–147.
Zaman, M.I., Mustafa, S., Khan, S., Xing, B., 2009. Effect of phosphate complexation on Cd2+ sorption by manganese dioxide (ß-MnO2). J. Colloid Interface Sci. 330 (1), 9–19.
Zeng, G., Wan, J., Huang, D., Hu, L., Huang, C., Cheng, M., Xue, W., Gong, X., Wang, R., Jiang, D., 2017. Precipitation, adsorption and rhizosphere effect: the mechanisms for phosphate-induced pb immobilization in soils? A review. J. Hazard. Mater. 339, 354–367.
Zhai, H., Wang, L., Qin, L., Zhang, W., Putnis, C.V., Putnis, A., 2018. Direct observation of simultaneous immobilization of cadmium and arsenate at the brushite-fluid interface. Environ. Sci. Technol. 52, 3493–3502.
Zhang, D., Chen, X., Larson, S.L., Ballard, J.H., Knotek-Smith, H.M., Ding, D., Hu, N., Fengxiang, X., Han, F.X., 2020. Uranium biomineralization with phosphate—biogeochemical process and its application. ACS Earth Space Chem. 4 (12), 2205–2214.
Zhang, G.Y., Peak, D., 2007. Studies of Cd(II)-sulfate interactions at the goethite water interface by ATR-FTIR spectroscopy. Geochim. Cosmochim. Acta 71 (9), 2158–2169.
Zhang, X., Huang, P., Zhu, S., Hua, M., Pan, B., 2019. Nanoconfined hydrated zirconium oxide for selective removal of Cu(II)-carboxyl complexes from high-salinity water via ternary complex formation. Environ. Sci. Technol. 53 (9), 5319–5327.
Zhao, L., Ding, Z., Sima, J., Xu, X., Cao, X., 2017. Development of phosphate rock integrated with iron amendment for simultaneous immobilization of zn and Cr(VI) in an electroplating contaminated soil. Chemosphere 182, 15–21.
Zhu, J., Cozzolino, V., Fernandez, M., Sánchez, R.M.T., Pigna, M., Huang, Q., Violante, A., 2011. Sorption of cu on a fe-deformed montmorillonite complex: effect of pH, ionic strength, competitor heavy metal, and inorganic and organic ligands. Appl. Clay Sci. 52, 339–344.
Zhu, J., Cai, Z., Su, X., Fu, Q., Liu, Y., Huang, Q., Violante, A., Hu, H., 2015. Immobilization and phytotoxicity of Pb in contaminated soil amended with γ-polyglutamic acid, phosphate rock, and γ-polyglutamic acid-activated phosphate rock. Environ. Sci. Pollut. R. 22, 2667.
Zhu, J., Fu, Q., Qiu, G., Liu, Y., Hu, H., Huang, Q., Violante, A., 2019. Influence of low molecular weight anionic ligands on the sorption of heavy metals by soil constituents: a review. Environ. Chem. Lett. 17, 1271–1280.
Zhu, R., Li, M., Ge, F., Xu, Y., Zhu, J., He, H., 2014. Co-sorption of cd and phosphate on the surface of a synthetic hydroxyiron-montmorillonite complex. Clay Miner. Miner. 62 (2), 79–88.
Zhu, Y., Elzinga, E.J., 2015. Macroscopic and spectroscopic assessment of the cosorption of Fe(II) with As(III) and As(V) on Al-oxide. Environ. Sci. Technol. 49 (22), 13369–13377.